Paleoceanography and Paleoclimatology

RESEARCH ARTICLE
10.1029/2025PA005245

Terrestrial Regulation of Lacustrine Hg Deposition During Glacial-Interglacial Cycles

Alice R. Paine[1,2], Joost Frieling[1,3], Bernd Wagner[4], Alexander Francke[5], Jack H. Lacey[6], Tamsin A. Mather[1], Stuart A. Robinson[1], and David M. Pyle[1]

[1]Department of Earth Sciences, University of Oxford, Oxford, UK, [2]Now at: Department of Environmental Sciences, University of Basel, Basel, Switzerland, [3]Now at: Department of Geology, Ghent University, Ghent, Belgium, [4]Institute of Geology and Mineralogy, University of Cologne, Cologne, Germany, [5]Discipline of Earth Science, School of Physics, Chemistry, and Earth Sciences, College of Science, Adelaide University, Adelaide, SA, Australia, [6]National Environmental Isotope Facility, British Geological Survey, Nottingham, UK

Abstract Mercury (Hg) is a toxic trace metal. It is clear that its natural cycle has been highly disturbed by human activities, but there remains much to understand about how it operated before these perturbations. For example, the influences of glacial-interglacial climate changes on the geochemical cycle of environmental Hg remain poorly understood. While key Hg surface reservoirs are sensitive to millennial-scale climate variations, it is unclear whether these responses influence their long-term behavior. Here, we explore how the terrestrial Hg cycle responds to environmental changes over multiple glacial-interglacial cycles by analysis of a ∼1.36-million-year-long sedimentary Hg record from the ancient Lake Ohrid (SE Europe): with the objective of understanding which processes may impact the behavior of this cycle on millennial timescales. Our analysis reveals periodic behavior in Hg between 1,360 and 780 thousand years ago (ka), but a weaker link from ∼780 ka to present. This transition corresponds roughly to the Mid-Pleistocene transition (MPT), which is observed in climate and ice-volume proxies in both Northern and Southern Hemispheres. These data confirm that long lacustrine Hg records are modulated by, and can capture variability in, terrestrial reservoirs for Hg. We propose that the change in Hg behavior corresponds to a reduction in catchment vegetation and soil carbon, and, consequently, Hg reservoir capacity following the Mid-Pleistocene transition. Our findings demonstrate that climate-driven changes in terrestrial reservoir size and stability can significantly influence the long-term behavior of Hg, which could have major implications for our understanding of this cycle on a regional to global scale.

Key Points:

- A ∼1.36-million-year-long sedimentary Hg record from the ancient Lake Ohrid (SE Europe)
- After ∼780 ka, there is a reduction in glacial-interglacial contrast between Hg values, which diverge from other ecological proxies
- Our data confirm that long lacustrine Hg records are modulated by, and can capture variability in, terrestrial reservoirs for Hg

Supporting Information:

Supporting Information may be found in the online version of this article.

Correspondence to:

A. R. Paine,
alice.paine@unibas.ch

Citation:

Paine, A. R., Frieling, J., Wagner, B., Francke, A., Lacey, J. H., Mather, T. A., et al. (2026). Terrestrial regulation of lacustrine Hg deposition during glacial-interglacial cycles. *Paleoceanography and Paleoclimatology*, *41*, e2025PA005245. https://doi.org/10.1029/2025PA005245

Received 16 JUN 2025
Accepted 9 MAR 2026

Author Contributions:

Conceptualization: Alice R. Paine, Joost Frieling, Tamsin A. Mather, Stuart A. Robinson, David M. Pyle
Data curation: Alice R. Paine
Formal analysis: Alice R. Paine, Joost Frieling
Funding acquisition: Bernd Wagner, Tamsin A. Mather
Investigation: Alice R. Paine, Joost Frieling
Methodology: Joost Frieling, Tamsin A. Mather
Project administration: Tamsin A. Mather
Resources: Bernd Wagner, Alexander Francke, Jack H. Lacey

1. Introduction

Mercury (Hg) is a toxic metal released into the atmosphere by both natural and anthropogenic processes (Obrist et al., 2018). Following removal from the atmosphere, Hg is cycled between major surface reservoirs (e.g., air, water, biomass), before eventually being sequestered in sedimentary archives, including marine and lake sediments, and soils. Studying the long-term evolution of this cycle is valuable for two reasons: (a) to assess the extent to which it may be influenced by different environmental processes and/or events, and (b) to constrain the "baseline" Hg cycle conditions that existed prior to human influence. Both are critical for building comprehensive models of Earth's system responses to climate variability, and can be used to directly assess the efficacy of recent regulatory action on biological Hg concentrations and human exposure (Outridge et al., 2018). However, due to the scale of modern anthropogenic pollution, and a scarcity of pre-Holocene studies, the natural background variability of the (terrestrial) Hg cycle and the processes driving variability in this cycle on geological timescales ($>10^3$ years) remain poorly understood (Amos et al., 2014; Selin, 2009). By testing hypotheses of Hg behavior in specific conditions and settings, we can begin to isolate key processes within the Hg source-to-sink pathway, and the extent to which this pathway may be influenced by, for example (hydro-) climate, ice cover, and ecosystem perturbations. Specifically, vegetation and soils are large surface reservoirs that hold organic matter and Hg, and are considered critical to the long-term ($\geq 10^2$ years) Hg cycle (Gworek et al., 2020). However, data to test the Hg cycle response to climate-driven changes in these two reservoirs are lacking.

Paleoclimate archives document over 40 transitions between glacial (cold) and interglacial (warm) conditions since 2.58 Ma (Palacios et al., 2022). These cycles operated with an obliquity-driven, 41-kyr periodicity prior to ∼1,200 ka, but after the Mid-Pleistocene Transition (MPT; ∼1,200–700 ka), they shift to a periodicity equating to ∼100-kyr. This led to the establishment of larger continental ice sheets in the Northern Hemisphere, and marked a

Supervision: Tamsin A. Mather, Stuart A. Robinson, David M. Pyle
Validation: Bernd Wagner
Visualization: Alice R. Paine
Writing – original draft: Alice R. Paine
Writing – review & editing: Alice R. Paine, Joost Frieling, Bernd Wagner, Alexander Francke, Jack H. Lacey, Tamsin A. Mather, Stuart A. Robinson, David M. Pyle

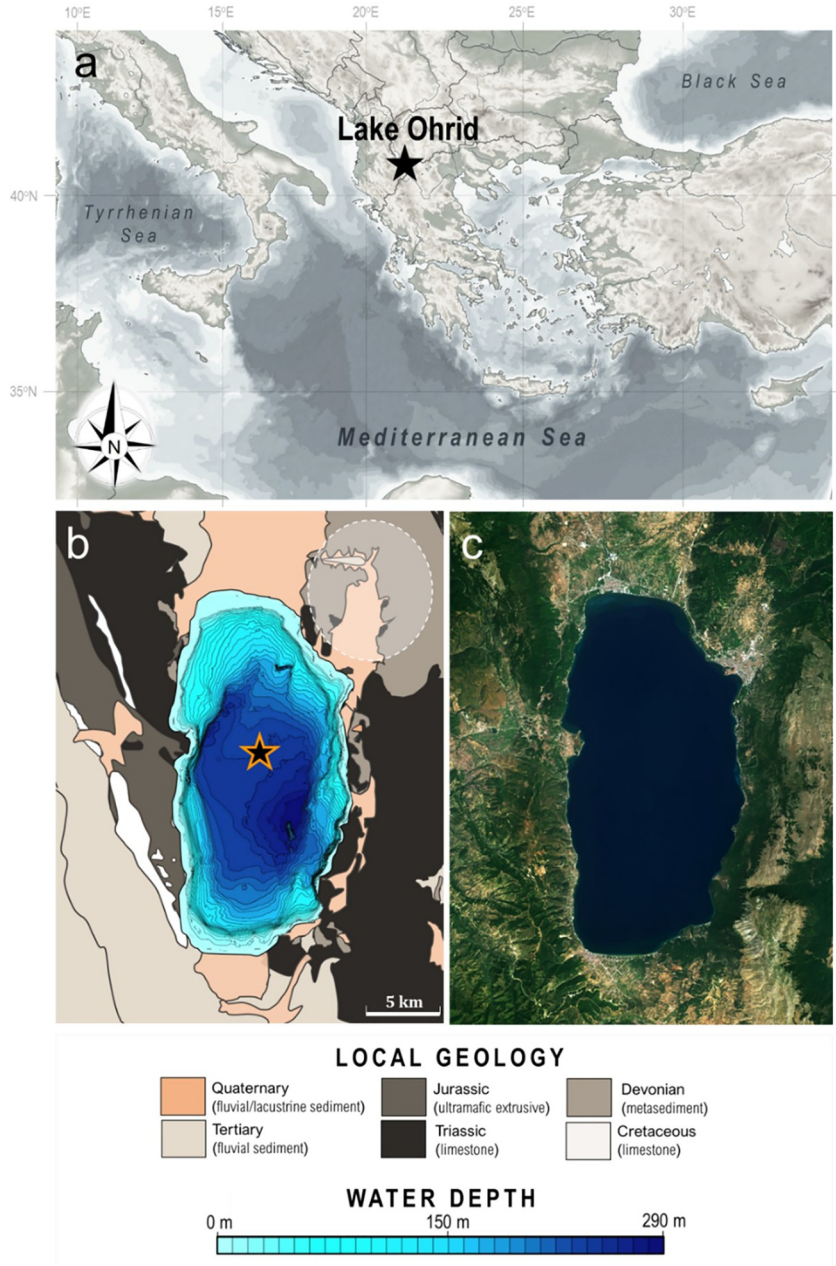

Figure 1. (a) Map showing the location of Lake Ohrid (41°02′N, 20°43′E) in south-east Europe, marked by a black star. (b) Bathymetric map of Lake Ohrid marked with 10-m contour intervals, and the 5045-1 (DEEP) drill site as a black, orange outlined star (Wagner et al., 2019). The dashed white oval marks an area of hydrothermal activity characterized by solfataras and fumaroles (Hoffmann et al., 2010). (c) Satellite image of the modern-day Lake Ohrid, where mixed forest can be seen surrounding the lake basin (© NASA 2022).

fundamental change in the Earth system (Clark et al., 2006). Glacial terminations occurred at specific points in the orbital configuration, when changes in (mid-latitude) insolation interrupted ice sheet expansions, prompting a return to warmer and wetter conditions (Palacios et al., 2022). Accompanying these climatic changes were significant modifications to ecosystem composition, structure, and functionality, manifesting as shifts in vegetation density, diversity, and interactions, and/or alterations in soil physical or chemical properties (Donders et al., 2021; Tzedakis et al., 2006). Physical glacial-interglacial changes in environmental conditions were also accompanied by changes in biogeochemical cycling. Global carbon (Yu et al., 2023), nitrogen (Ren et al., 2017) and phosphorus (Filippeli, 2008) cycles all follow a characteristic "sawtooth" pattern in many late Pleistocene:

records reflecting the consequences of a gradual cooling trend from glacial inception to peak glacial conditions, followed by a rapid glacial termination.

The limited evidence that is available suggests glacial-interglacial changes in Hg may follow a similar pattern to the Quaternary glacial-interglacial climate variations. For example, clear increases in Hg concentrations are documented during the last deglaciation (*termination I:* 19–11 ka) in ice cores (e.g., Segato et al., 2023) and terrestrial (lacustrine) sediments (e.g., Paine et al., 2024). Knowledge of Hg cycle variability spanning further back into the Pleistocene is based almost entirely from records produced from marine sediment cores, which document low-amplitude shifts in Hg concentration proposed as corresponding to oscillations in atmospheric and ocean circulation during the last glacial cycle (Chede et al., 2022; Figueiredo et al., 2022). However, these longer records are controlled by both marine and terrestrial processes, making it difficult to isolate the influences of specific processes and source-to-sink Hg pathways. Hence, it also remains unclear whether the changes related to glacial-interglacial transitions produce regular variations in marine or terrestrial Hg records, and which, if any, processes may control this behavior.

Here, we present a 1,360-kyr-long sedimentary Hg record using the Lake Ohrid sediment succession (Figure 1) that continuously covers the entire lake history up to the present day. Lake Ohrid has an exceptional paleo-environmental framework with which to examine Hg variability relative to changing local conditions, and records both tectonic and climate-driven changes in sedimentation (Wagner et al., 2019). Therefore, these sediments record glacial-interglacial cyclicity both prior to and following the MPT, and offer the opportunity to explore if sedimentary Hg responds to both orbital-scale climate changes, and regional-to-global-scale biogeochemical processes.

2. Study Setting

Lake Ohrid (41°02′N, 20°43′E) is a tectonic lake situated 693 m above sea level in south-east Europe (Figure 1a). The present-day lake is ∼30 km long, 15 km wide and up to 293 m deep, with a ∼1,300 km^2 catchment. The lake lies in the hydrothermally active Korça-Ohrid earthquake source zone (Hoffmann et al., 2010), with Quaternary lacustrine and fluvial deposits on the northern and southern plains, and mountain ranges to the west and the east of the basin (Figure 1b, Figure S1 in Supporting Information S1). Vegetation and soil types in the modern-day Ohrid catchment are distributed in altitudinal belts. Mixed deciduous forests and rendzina (organic-rich) soils are typically found in lower-elevation regions (<1,800 m), whereas in the higher montane areas sub-alpine grasses, beech and coniferous forests, and acidic podzolic soils are more common (Figure 1c; Vogel et al., 2010). The ∼447 m-long sedimentary succession extracted from the DEEP (central) site provides a continuous record of hemipelagic sediment accumulation since ∼1,360 ka, with age control provided by combining tephrochronological data from 16 ^{39}Ar/^{40}Ar dated tephra layers, magnetostratigraphic data, and orbital-tuning of peaks in total organic carbon (TOC, Figure S2 in Supporting Information S1; Wagner et al., 2019). The 95% confidence intervals of ages for specific depths produced by Bacon Bayesian age modeling are ±5.5 kyr on average, with a maximum of ±10.6 kyr (Text S2 in Supporting Information S1). Detailed description of the parameters and software used to construct the final age-depth model is included in a Supporting Information S1 file.

3. Methods

3.1. Sedimentary Mercury

Paine et al. (2024) analyzed sedimentary Hg concentrations in the top 36 m of the DEEP 5045-1 sediment succession. We extend this data set to cover the full ∼447 m succession, with Hg measurements taken for 640 powdered bulk sediment samples between ∼36 and ∼447 m composite depth at a sampling resolution of 64 cm (or an average of ∼2 kyr). Total Hg concentrations (Hg_T) were measured using a RA-915+ Portable Mercury Analyzer with PYRO-915+ Pyrolyser, Lumex (Bin et al., 2001) at the University of Oxford. Powdered samples (39–340 mg mass) were weighed into glass measuring boats, placed into the pyrolyser (*Mode 1*), and heated to ∼700°C. The Hg present is volatilized and oxidized to Hg^0 and quantified via spectral absorption, and the instrument subsequently records the absorption of UV light by Hg atoms at a specific wavelength: signaling the total Hg content of the sample (Bin et al., 2001). Standard materials (paint-contaminated soil—NIST Standard Reference Material ® 2587) with a known Hg value of 290 ± 9 ng g^{-1} were run prior to and during sample analysis to calibrate the instrument. Analysis of repeated standard measurements (using masses tailored to give

comparable peak areas to the samples analyzed) indicate reproducibility is generally ±10% or better in line with long-term observations of this standard on this machine (Frieling et al., 2023).

Rates of Hg accumulation in both cores were calculated by:

$$Hg_{AR} = Hg_T\ (DBD \times SR) \quad (1)$$

where Hg_{AR} is the total Hg mass accumulation rate (mg m^{-2} kyr^{-1}), Hg_T is the total Hg concentration in a sample (mg g^{-1}), DBD is the dry bulk density (g m^{-3}), and SR is the sedimentation rate (m kyr^{-1}). Values for Hg_{AR} are calculated with respect to the median age estimate for each sample. Sedimentation rate values are those calculated by Wagner et al. (2019), see also SI 2). Dry bulk density values were calculated immediately after sampling from volumetrically sampled aliquots at the University of Cologne (Francke et al., 2016).

To explore whether sedimentary Hg is present in a single or multiple host-phases, thermal desorption profiles (TDPs) were obtained for a representative subset of 5045-1 samples ($n = 29$) using the continuous-flow-based methodology presented in Frieling, Fendley, et al. (2024) (Table S1 in Supporting Information S1). Samples at room temperature were rapidly heated to 700°C, with Hg release lasting typically <1 min. Both Hg_T and TDPs for each sample were obtained simultaneously using a Lumex RA-915M at the University of Oxford, with a detector signal at one second increments extracted from the raw time-series output. The raw thermal desorption data for each sample were isolated from the detector time series using the sample start and end point flags as recorded in the Lumex RAPID software. Similar to total Hg concentration measurements, all Hg TDPs were obtained in the highest-temperature mode, without boost heating. The weight of each sample was held constant (50 ± 4 mg) to limit any effects of thermal inertia during sample heating and ensure reproducibility (Frieling, Fendley, et al., 2024; Frieling, Mather, et al., 2024).

3.2. Carbonate Correction

In Lake Ohrid, endogenic calcite ($CaCO_3$) accounts for up to >80% of the total sediment carbonate mass with small contributions from biogenic and detrital terrigenous calcium carbonate (Lacey et al., 2016), and is generally most dominant during warm, interglacial periods (Wagner et al., 2019). Such a high and variable carbonate content creates a high risk of Hg fluxes to the sediment being diluted, and the variability results in a positive correlation to other diluted phases (TOC, TS, quartz, clay minerals), when this effect is not suitably accounted for. Carbonate-dilution is a common feature in sedimentary Hg records, as carbonate minerals rarely host appreciable amounts of Hg (Fendley et al., 2024). As carbonate accumulation increases, Hg-bearing siliciclastic or organic components can be diluted to such an extent that it produces a "false" reduction in Hg concentrations—a reduction that may be incorrectly interpreted as a change in net Hg flux to the system. Indeed, we observe a negative correlation between total inorganic carbon (TIC) and Hg_T ($r^2 = 0.64$, $r = -0.8$) that indicates carbonate dilution exerted a significant effect on Hg concentrations throughout the DEEP 5045-1 record (Figure S3 in Supporting Information S1).

The dilution effect imposed on Hg_T in this system also extends to other non-carbonate compounds such as organic and siliciclastic detrital material (Figure S3 in Supporting Information S1). TOC appears the least affected by this dilution, probably because more intense authigenic carbonate precipitation in warm interglacial periods coincides with higher primary productivity and TOC contents in the sediments (Francke et al., 2016).

To remove the correlation imprinted by carbonate dilution on organic and detrital compounds in DEEP 5045-1, and to avoid spurious correlations between Hg and any other parameters, or periodicity imprinted by carbonate dilution we assess Hg, organic matter (TOC), and detrital (Qz, K) variations on a carbonate-free basis (CFB). We use:

$$X_{CFB} = \frac{X}{1 - \frac{CaCO_3}{100}} \quad (2)$$

where X indicates values for Hg_T, TOC, K, and Qz, and X_{CFB} represents the carbonate-free concentration/abundance of each species, respectively. $CaCO_3$ is the concentration (wt %) of calcium carbonate in a given sample. Concentrations of $CaCO_3$ are calculated from TIC according to the mass ratio using:

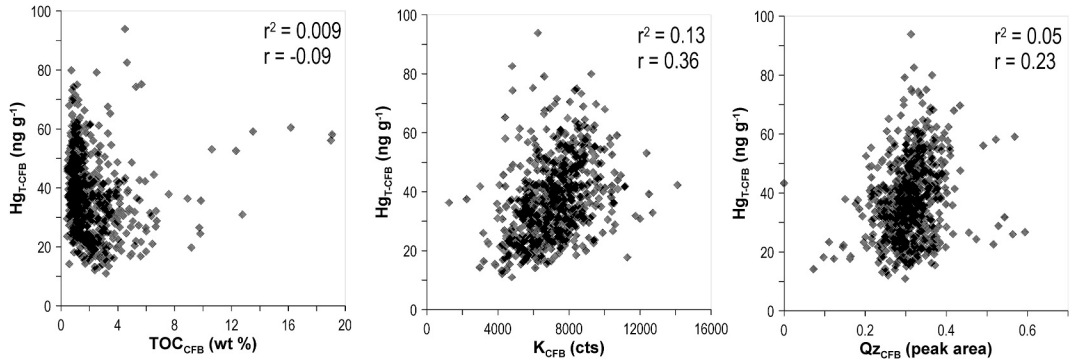

Figure 2. Comparison of the relationship between $Hg_{T\text{-}CFB}$ and Qz_{CFB}, $Hg_{T\text{-}CFB}$ and K_{CFB}, and $Hg_{T\text{-}CFB}$ and TOC_{CFB}—all corrected for carbonate dilution. R-squared (r^2) and r values are also included. All correlations ($n = 640$) are significant at $p < 0.01$ but never explain a substantial proportion of the variability.

$$CaCO_3 = TIC \times 8.33 \quad (3)$$

drawing upon published TIC values (Wagner et al., 2019). Inorganic carbon compounds in the Lake Ohrid sediment archive are dominated by calcite with minor amounts of siderite ($FeCO_3$) present during periods of overall low TIC (Lacey et al., 2016). As $CaCO_3$ is by far the dominant form we here assume all TIC is in $CaCO_3$ (Equation 3) to correct for carbonate dilution. The parameters Qz_{CFB} and K_{CFB} are practical metrics, where the relation with carbonate is removed. However, due to the potential influence of non-linearities in the X-Ray Fluorescence (XRF) and Fourier Transform Infrared Spectroscopy (FTIR) analyses that underlie K and Qz data, these K_{CFB} and Qz_{CFB} data should not be interpreted quantitatively. They are simply used to test for potential co-enrichment of Hg, K and Qz outside the influence of carbonate dilution.

3.3. Time Series Analysis

To test whether cycles of significant spectral density are present in the DEEP 5045-1 Hg record, we performed Lomb-Scargle spectral analysis using PAST v.4.16 software (Hammer et al., 2001). Low coefficient values produced by an autoregressive moving average (ARMA) model (Table S3 in Supporting Information S1) suggest that the data lacks strong temporal dependencies that would infer a strong red-noise influence (e.g., van der Bolt et al., 2018), does not contain any major gaps, was sampled at regular depth intervals, and reflects a relatively stable sedimentation rate (Francke et al., 2016; Wagner et al., 2019). To ensure our interpretation of the Hg record was independent, and so avoid assumptions based on Hg behavior itself, we sub-divided the time-series into three intervals prior to assessing spectral power. This subdivision followed preliminary identification of a dominant periodicity of ~1,086-kyr in the full (~1,360–0 ka) DEEP 5045-1 $Hg_{T\text{-}CFB}$ data set, which suggests interference from a non-environmentally significant factor (Figure S8 in Supporting Information S1). Thus, the data was divided based on objective changes in lake history and global boundary conditions, notably the onset of hemi-pelagic sedimentation (1,360–1,200 ka), establishment of oligotrophic conditions (1,200–780 ka), and global shift to ~100-kyr glacial cycles (780–0 ka) (Wagner et al., 2019). These time-windows also aid the examination of local Hg behavior evolution across the MPT.

Frequency values in cycles/kyr of the Lomb–Scargle periodograms were transferred into the time-domain ($Freq_{TIME}$) to indicate the statistically relevant cycles in kiloyears (kyr), using

$$Freq_{TIME} = 1/(F) \quad (4)$$

where F is the frequency value generated by the spectral analysis.

The temporal evolution of dominant periodicities in the data was explored first by continuous wavelet transform (CWT) analysis, using a Morlet mother wavelet. Red-noise background was corrected for autocorrelation by applying an autoregressive moving average (ARMA) to the data series, following which a wavelet power spectrum was computed. Spectral analysis of the detrended $Hg_{T\text{-}CFB}$ data was performed first on the full

(~1,360–0 ka) series, and subsequently on three discrete intervals based on changes in lake history (1,360–1,200 ka, 1,200–780 ka, and 780–0 ka).

To isolate periodicities associated with cycles identified as significant (~41 and ~100 kyr) in the Lomb-Scargle spectral analysis we applied a bandpass filter to the DEEP 5045-1 $Hg_{T\text{-}CFB}$ data using the R package *astrochron* (Meyers, 2014). Bandpass analyses were conducted on the raw, non-detrended, $Hg_{T\text{-}CFB}$ data using frequency ranges of 38–46 kyr and 90–130 kyr to extract variability associated with the 41 and 100 kyr cycles respectively. These frequency ranges were calculated to accommodate the dominant frequencies, and allow some stretching around that frequency to minimize impact from small errors introduced by the age-depth model. Mean cycle duration for each orbital configuration following the orbital solution of Laskar et al. (2004) (Table S4 in Supporting Information S1). Higher frequency periodicities that might be associated with astronomical precession (~19–24 kyr) were not significant anywhere in the power spectra (Figure 4), and so are not included in bandpass analyses.

4. Results

Reconstruction and comparison of Hg variability within the DEEP sediment succession requires isolating Hg variability from variations associated with organic carbon (e.g., represented by TOC), and detrital phases (e.g., represented by Qz, K). Although many previous studies have normalized Hg concentrations to these, this approach also imprints the variability of those parameters on the normalized Hg ratio, and may mask subtle variability in Hg.

Near-zero correlation coefficients between $Hg_{T\text{-}CFB}$ and carbonate-corrected proxies for organic-matter and detrital materials suggest that, after removing the carbonate dilution effects, Hg variability is generally unrelated to the availability of both organic and detrital host phases (Figure 2). There is no evidence for co-enrichment of Hg and TOC, Qz or K across the full data set (Figure S5 in Supporting Information S1), and throughout the time interval covered by the DEEP core (Figure S6 in Supporting Information S1). Although these correlations reach statistical significance (likely due to large sample size; $n = 640$), their explanatory power is very limited as Qz/K and TOC account for only ~1%–5%, and <1% of the variance in Hg, respectively (Figure 2). This extremely low co-variance, therefore, suggests that host-phase influences are minor relative to other processes. This is significant for two reasons. First, it suggests that normalizing $Hg_{T\text{-}CFB}$ to any of these phases (whether in carbonate-free space or bulk) would be inappropriate, as it would effectively imprint variability in these phases onto the Hg-normalized parameter, and so introduce artifacts to the data set. Second, it implies that normalizing Hg to K, Qz, or TOC (bulk or carbonate-corrected) would not remove any co-enrichment effects such as may be common in the marine realm (Shen et al., 2020). Indeed, prior to applying a normalization a strong linear relation with a zero intercept ($y = a \times x$) needs to be demonstrated to avoid introducing major errors, and biasing such as inflation of Hg-normalized values at low "host phase" abundance. These basic prerequisites are not met here (Figure 2). Instead, Hg normalization would imprint the unrelated variability in other phases onto Hg, introducing artifacts. We consider $Hg_{T\text{-}CFB}$ as the most appropriate parameter to examine (isolated) Hg variability.

The sediments of core DEEP 5045-1 record clear variability in $Hg_{T\text{-}CFB}$ through time (Figure 3a). $Hg_{T\text{-}CFB}$ values average 37.4 ng g^{-1} (range: 10.9–93.9 ng g^{-1}, standard deviation: 13.2), with the largest peaks recorded between ~260 and 130 ka. Accumulation rates (Hg_{AR}) average 10.7 mg m^{-2} kyr^{-1} (range, 0.7–42.6, standard deviation 7.7 mg m^{-2} kyr^{-1}), and the largest Hg_{AR} peaks are also concentrated between ~260 and 130 ka, when sedimentation rates also reach maximum values (Figure 3g).

The absence of a correlation between Hg, common sedimentary host phases (e.g., TOC), or clastic detrital matter (e.g., Qz, K) might also suggest that variability in the Hg flux to the lake dominates the Hg deposition, or that more unusual and/or variable host-phases obscure the Hg-host phase relation. We test whether any Hg speciation changes occur by analyzing thermal desorption profiles (TDPs) of representative samples through the sequence, and these profiles reveal a single, dominant phase (that contains >90% of Hg) in all samples (Figure S7 in Supporting Information S1). Organic-matter associated Hg is the most common form upon deposition and, given the low overall concentrations of sulfur in DEEP 5045-1, it is therefore likely that this single TDP phase reflects an organic phase that contains (almost all) Hg. This is further supported by the observation that organic-bound Hg in natural sediments generally desorbs at low temperatures relative to other, more thermally stable, materials (e.g., sulphides, iron hydroxy complexes and more exotic Hg minerals) (Frieling, Fendley, et al., 2024; Frieling, Mather, et al., 2024; Saniewska & Bełdowska, 2017). Together with the lack of evidence that host-phase

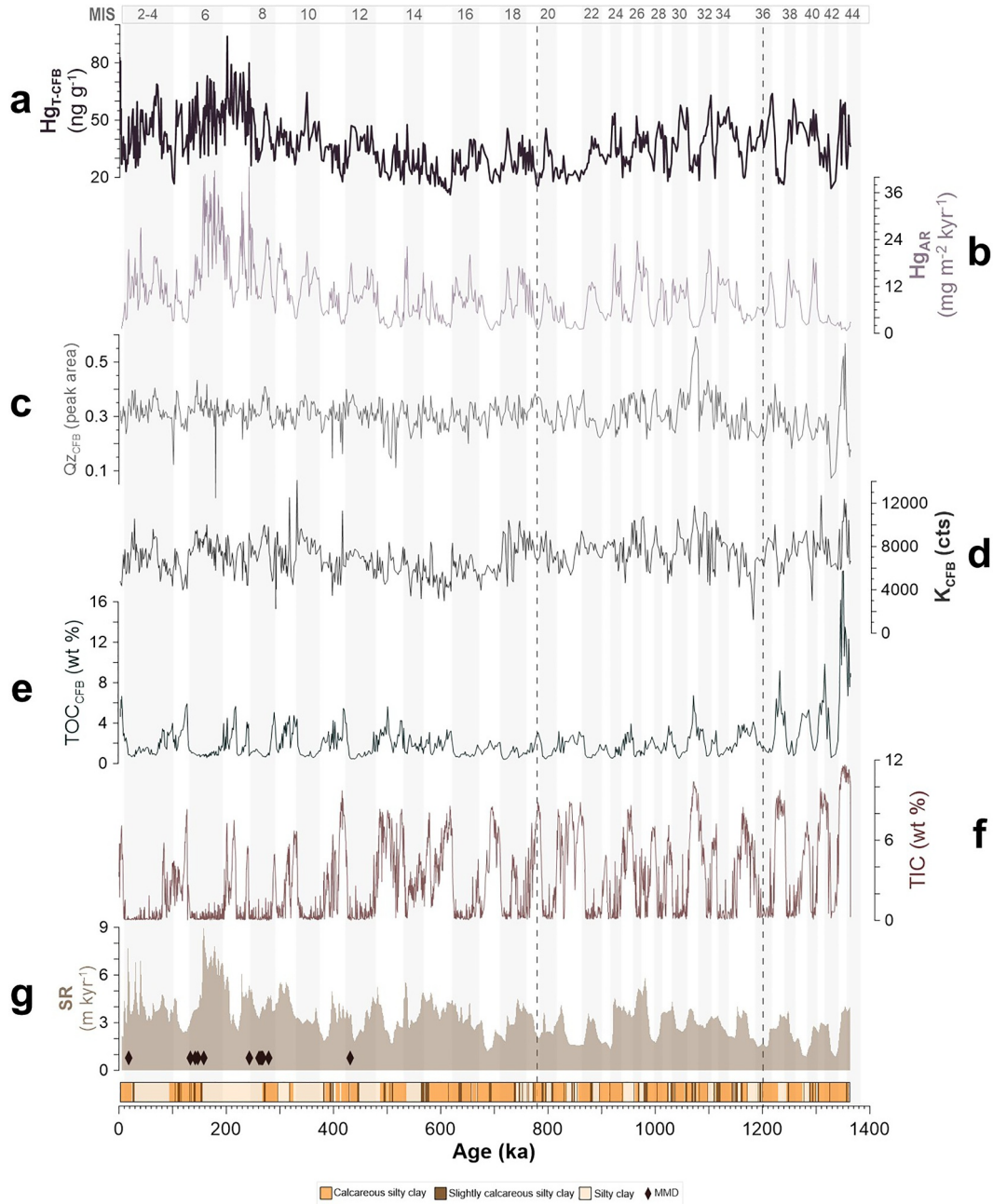

Figure 3. Sedimentological data obtained from core DEEP 5045-1. (a) Total Hg ($Hg_{T\text{-}CFB}$), (b) Hg accumulation rate (Hg_{AR}), (c) quartz abundance (Qz), (d) potassium abundance (K), (e) total organic carbon (TOC), (f) total inorganic carbon (TIC) concentrations, (g) sedimentation rate (SR) is calculated from published chronology and grain-size information (data sets (c–g) first presented in Wagner et al. (2022, 2019). Mass movement deposits (MMD) are marked by brown diamonds (Francke et al., 2016), and lithological data based on published literature (Wagner et al., 2019). Glacial intervals are marked by gray bars based on the Marine Isotope Stage (MIS) stratigraphy (Lisiecki & Raymo, 2005). Dashed vertical lines mark the boundaries of three key intervals in the lake's history and global boundary conditions: 1,360–1,200 ka (onset of hemipelagic sedimentation), 1,200–780 ka (establishment of oligotrophic conditions), and 780–0 ka (global shift to ~100-kyr glacial cycles) (Wagner et al., 2019).

abundance exerts any appreciable control on sedimentary Hg content both in bulk, and with carbonate dilution effects included (Figure 2, Figure S5 in Supporting Information S1), we infer that the net Hg supply is the first-order control on $Hg_{T\text{-}CFB}$ and Hg_{AR}. Similar "flux-limited" regimes have been observed in other lacustrine

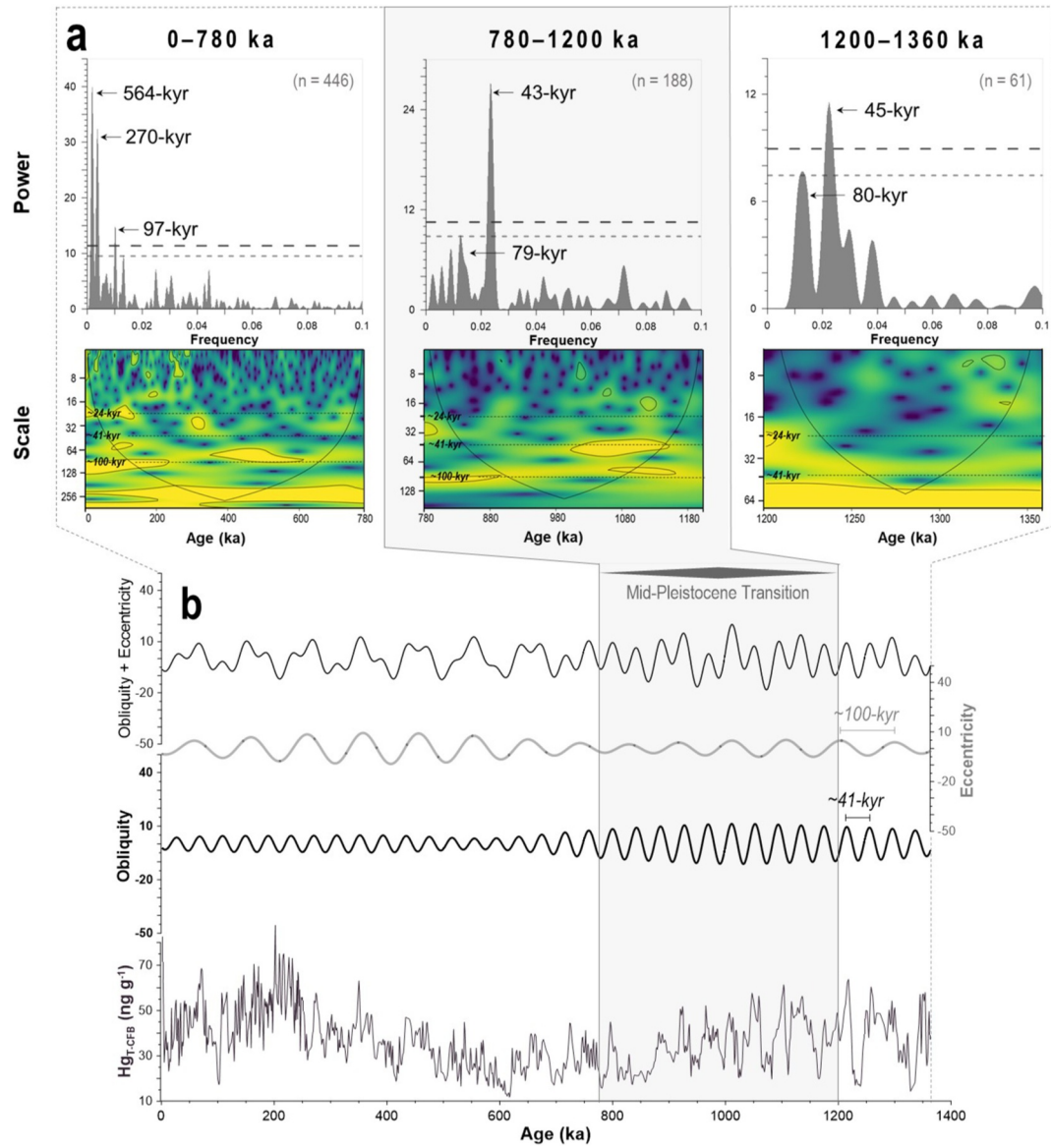

Figure 4. Spectral analysis results for DEEP 5045-1. (a) Lomb-Scargle periodograms for three discrete intervals in the DEEP 5045-1 core: ~1,360–1,200 ka, ~1,200–780 ka, <780 ka show significant ($p < 0.01$) periodicities in each of the three data sets. Horizontal dashed lines mark $p < 0.01$ (dark gray, large dashes) and $p < 0.05$ (light gray, small dashes) significance levels. Also shown are scalograms that present the results of continuous wavelet transform (CWT) analysis. The *y*-axis is a logarithmic size scale (base 2) whereby one unit corresponds to a doubling of the size scale; note the *y*-axes are different for the three time-slices. Black contours indicate coherence above the 95% significance level against red-noise background, corrected for autocorrelation. Color bars indicate the power of wavelet coherence whereby yellow marks the highest power. (b) Bandpass filters (dark blue lines) that isolate components in the DEEP data set related to the obliquity (38–46 kyr) and short eccentricity (90–130 kyr) cycles.

environments (Paine et al., 2024), and appear different from many marine systems in which host phase availability seems to more often control Hg drawdown (Shen et al., 2020).

Between 1,360 and 780 ka, the Hg_{T-CFB} data shows a significant ($p < 0.01$) ~43 to 45-kyr (obliquity) periodicity with particularly strong coherency between 1,200 and 780 ka (Figure 4). These ~44-kyr peaks in Hg_{T-CFB} typically correspond to glacial intervals characterized by deposition of sediments containing low TOC_{CFB} (<1 wt%; Figure 3e), and arboreal pollen concentrations (Figure 5b); signaling low aquatic productivity and catchment vegetation density, respectively (Francke et al., 2016; Wagner et al., 2019). Conversely, troughs in

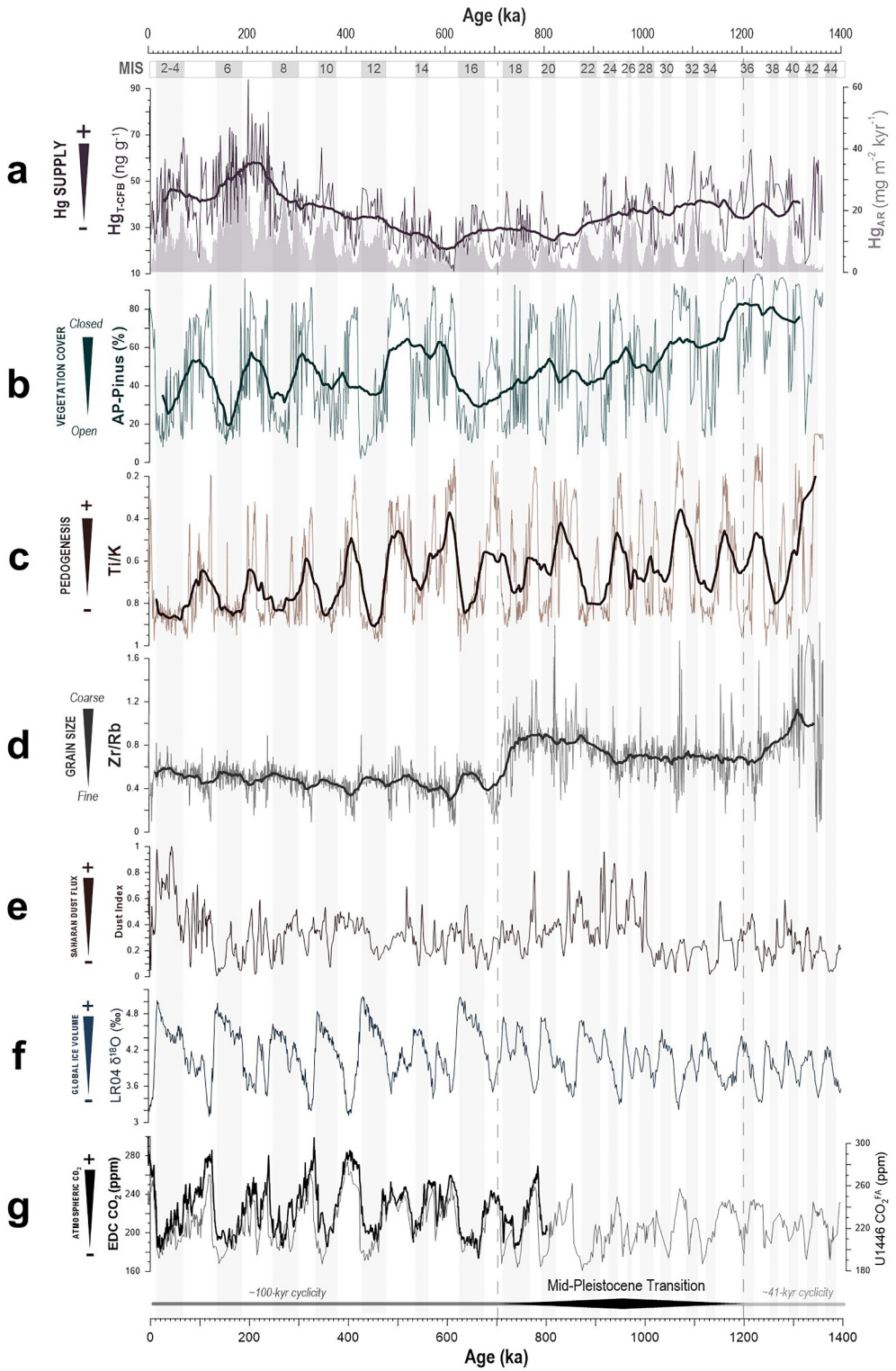
Age (ka)
0 200 400 600 800 1000 1200 1400
MIS 2-4 6 8 10 12 14 16 18 20 22 24 26 28 30 32 34 36 38 40 42 44
a
Hg SUPPLY
+
-
$Hg_{T\text{-}CFB}$ (ng g^{-1})
Hg_{AR} (mg m^{-2} kyr^{-1})
b
VEGETATION COVER
Closed
Open
AP-Pinus (%)
c
PEDOGENESIS
Ti/K
d
GRAIN SIZE
Coarse
Fine
Zr/Rb
e
SAHARAN DUST FLUX
Dust Index
f
GLOBAL ICE VOLUME
LR04 $\delta^{18}O$ (‰)
g
ATMOSPHERIC CO_2
EDC CO_2 (ppm)
U1446 CO_2^{FA} (ppm)
~100-kyr cyclicity
Mid-Pleistocene Transition
~41-kyr cyclicity
Age (ka)

Figure 5.

$Hg_{T\text{-}CFB}$ seemingly correspond to interglacial intervals, characterized by high TOC_{CFB} (>2 wt%; Figure 3e) and arboreal pollen concentrations (Figure 5b), coupled with minimal influx of detrital materials (Figures 2 and 5).

Glacial-interglacial variations in Hg show a fundamental shift at ~780 ka: corresponding to the later stages of the MPT (~1,200–700 ka). This shift is characterized first by a visible reduction in the amplitude of $Hg_{T\text{-}CFB}$ signals between glacial and interglacial intervals (Figure 2), which is also captured in the DEEP spectral analysis (Figure 4). Specifically, by weakening of periodicity in the obliquity (~41-kyr) band in the 780–0 ka period, which is only partially compensated by the emergence of a subtle, lower (~97 kyr) frequency cycle (Figure 4). This behavior is not shown by TIC and deciduous oak in the same interval, which both continue to show clear, orbitally coherent, ~100-kyr cyclicity between ~780 and 0 ka (Wagner et al., 2019).

A second feature of the reduction in $Hg_{T\text{-}CFB}$ cyclicity at ~780 ka is the fact this reduction does not occur in other organic, detrital, and mineral indicators within the DEEP sediments (Figures 5b–5e). These other indicators all clearly document the progression from ~41-kyr to ~100-kyr glacial-interglacial cycles across the MPT (Clark et al., 2006). For example, arboreal pollen measurements suggest that glacial-interglacial cyclicity in local vegetation was not only retained following the MPT, but also tracked the global-scale transition from ~41 to ~100-kyr climate cycles (Figure 5b; Donders et al., 2021; Francke et al., 2016; Wagner et al., 2019). Variations in TIC and Ca/K also track this shift which, coupled with a step-shift to fine-grained sedimentation at the DEEP coring site beginning at ~760 ka (Figure 5d), pertain to major changes in local karst aquifer activity, aquatic productivity, and sediment deposition in the Ohrid basin as a systemic response to longer, and likely colder, glacial intervals (Wagner et al., 2019).

The evident lack of a dominant host-phase influence suggests that variability in $Hg_{T\text{-}CFB}$ in DEEP 5045-1 is most likely associated with Hg supply to Lake Ohrid (Figure 2). However, the reduction in $Hg_{T\text{-}CFB}$ cyclicity at ~780 ka also becomes increasingly dissociated from the broader (climate-driven) sedimentary changes occurring in Lake Ohrid during this time. Hence, this discrepancy suggests that additional processes influenced orbital-scale Hg behavior in the Ohrid system, providing a foundation from which to discuss other potential drivers of orbital-scale Hg cycling.

5. Discussion

5.1. Drivers of Orbital-Scale Mercury Cycling

Our ~1,360-kyr Hg record reveals two intriguing features. First, Hg variability appears to be driven by regular cyclicity at a ~41-kyr orbital frequency between ~1,360 and 780 ka (Figure 4). Second, the regular behavior observed in Hg is more coherent with orbital cycles prior to ~780 ka, while less of the Hg variability can be explained by such cycles ~780–0 ka (Figure 5). The reduction in the proportion of Hg signal variability that can be explained by orbital components following ~780 ka (Figure 4) is largely due to an increase in variability that does not clearly correspond to any orbital cycle (Figure 5). This reflects a response opposite to other organic, detrital, and mineral indicators within the DEEP sediments, which clearly document the progression from ~41 to ~100-kyr glacial-interglacial cycles across the MPT, and likely relate to major changes in local karst aquifer activity, aquatic productivity, and sediment deposition in response to longer, and likely colder, glacial intervals (Wagner et al., 2019). Two $^{39}Ar/^{40}Ar$-dated tephra layers also provide independent age control for the interval where the change in Hg behavior occurs (~780 ka): one at 715.02 ± 5.4 ka, and the second at 789.38 ± 1.9 ka (Leicher et al., 2021). This suggests that, even if we consider the average error margin within the DEEP 5045-1 core chronology (±10.6 kyr; Wagner et al., 2019), the $Hg_{T\text{-}CFB}$ shift still occurs well within the known temporal range of the corresponding climate, lithology and vegetation shift.

Figure 5. (a) Total Hg corrected for carbonate dilution ($Hg_{T\text{-}CFB}$), and Hg accumulation rate (Hg_{AR}) from core DEEP 5045-1. (b) Relative percentages of arboreal pollen (AP) excluding *Pinus*, *Betula*, and *Juniperus*-type genera (Donders et al., 2021). (c) Ti/K ratios as a proxy for soil development (low ratios imply increased supply of dissolved K, secondary clay minerals and thus well-developed soil structures (Francke et al., 2019). (d) Zr/Rb ratios as a proxy for grain size (higher ratios typically indicate greater contribution of coarse materials) (Wagner et al., 2022). (e) A normalized dust index generated from cores extracted at marine Ocean Drilling Program Site 927, offshore Cyprus (Grant et al., 2017). (f) Benthic foraminiferal calcite $\delta^{18}O$ (‰) (the LR04 stack) with cold glacial stages defined by high $\delta^{18}O$ ratios (Lisiecki & Raymo, 2005). (g) Atmospheric CO_2 from the EPICA Dome C ice core (Bereiter et al., 2015), CO_2 reconstruction from International Ocean Discovery Program Site U1446 from the Bay of Bengal (Yamamoto et al., 2022), and a record of Marine Isotope Stages (MIS) derived from the LR04 stack (Lisiecki & Raymo, 2005) and the Mid-Pleistocene Transition are also marked. Original data sets are presented by lighter lines, with an overlaying thicker line denoting the moving average of each data set (~50-kyr equating to 32 data points (on average).

We evaluate the potential origin of regular changes in Hg burial in the lake, considering three primary mechanisms: (a) the efficiency of burial relative to re-emission (evasion) within the lake itself, (b) the overall flux of Hg to the catchment from the atmosphere, and/or (c) flux modulation by reservoirs within the catchment. All three can be closely tied to climate, shift in response to glacial-interglacial transitions, and could therefore reflect the influence of both global-scale and local processes on this record. Furthermore, while all three mechanisms can impact Hg cycling across glacial-interglacial cycles, the frequency of variability and evolution in Hg response to glacial-interglacial changes through time may hold clues as to which was most important.

5.1.1. Changes in Mercury Burial Efficiency

In a lacustrine system, the long-term efficiency of Hg burial relative to evasion can be influenced by contrasting local environmental conditions during discrete climatic intervals. For example, extension of ice toward the middle of the basin during cold periods could cause a net reduction in the conversion rate of oxidized Hg species (Hg^{2+}) to elemental Hg (Hg^0) (photoreduction) on the lake surface and/or in the water column, while simultaneously decreasing evasion of "photoreductively available" Hg^0 back to the atmosphere (Clarke et al., 2023; O'Driscoll et al., 2018).

A growing body of research has shown that the signals encoded in lake sediment records over multiple millennia are likely influenced by a combination of processes originating within, and outside of, the lake basin itself (e.g., Bravo et al., 2017; Paine et al., 2024; Sahoo et al., 2023). Whilst the $Hg_{T\text{-}CFB}$ may be affected by, for example, sediment redox processes, the processes that occur during early diagenesis typically can only mobilize and displace Hg in the stratigraphy across very short (cm-scale) distances (e.g., Frieling et al., 2023; Gagnon et al., 1997). Moreover, to avoid the potentially misleading effects of variable siliciclastic input (Figure 2) and carbonate dilution (Figure S3 in Supporting Information S1), we also examine the $Hg_{T\text{-}CFB}$ and Hg_{AR} records in unison (Figures 3 and 5). Together with the limited long-term impact of diagenetic changes, the clearly synchronous fluctuations in these two time series' provide evidence that the system is subject to (true) burial flux changes on orbital time-scales (Figure 3).

Organic and/or detrital matter sedimentation may also trigger a change in lacustrine Hg burial efficiency (Kovács et al., 2024; Shen et al., 2020). Both sedimentation regimes show clear responsivity to glacial-interglacial scale cyclicity in Lake Ohrid (Figure 2) meaning that, if supply of Hg to the DEEP 5045-1 sediments was controlled solely by burial efficiency, the temporal evolution of Hg variability in this system would be expected to show the same clear glacial-interglacial contrast captured by other proxies in the succession (Figure 4). However, the total variation explained by obliquity- and eccentricity-driven periodicity in the $Hg_{T\text{-}CFB}$ curve is relatively reduced in the ~780–0 ka period, and this increasingly "noisy" pattern notably diverges from that observed in proxies such as TOC and Ti/K that represent primary (aquatic) productivity and soil formation (Figure 5). Taken together, this shift in Hg behavior suggests another factor, not directly or linearly corresponding to global or local glacial-interglacial trends, but also unrelated to solely burial efficiency, may have been more influential.

5.1.2. Changes in Atmospheric Fluxes

The overall flux of Hg to the catchment from the atmosphere presents a plausible cause of cyclic changes in Hg supply and ultimately Hg burial. During the Pleistocene, precession-controlled changes in aridity and wind strength drove intense dust mobilization from the Sahara desert (Figure 5e), and transport across the Mediterranean basin during glacial periods (Grant et al., 2017). Atmospheric dust transport also plays a critical role in the global dispersal of Hg (Huang et al., 2020; Qin et al., 2024), and several studies have attributed increases in the Hg concentration of materials deposited in marine and lake basins during glacials to enhanced dust fluxes (e.g., Fadina et al., 2019; Pérez-Rodríguez et al., 2018; Xue et al., 2025). Similar to burial efficiency (Section 5.1.1), we might therefore expect a certain regular pattern of the dust influx imposed on the deposition of Hg. Specifically, this mechanism might be recognized as a persistent precession, or eccentricity (through precession modulation), frequency cycle in Hg variability across the analyzed period. Yet, despite the presence of quasi-cyclic changes in the abundance of aeolian clastic material in the Ohrid sediments (Vogel et al., 2010), $Hg_{T\text{-}CFB}$ and Hg_{AR} show a limited overall influence of the eccentricity-frequency cycle (only after 780 ka) and no significant precession forcing (Figure 4). That said, we cannot rule out the potential for smoothing, overprinting, and/or redistribution of Hg signals in the lake sediments relative to the original dust flux by the diverse range of processes known to affect Hg stored in soils, vegetation, or surface sediments (Bishop et al., 2020). The Hg

signals preserved in Lake Ohrid may reflect an integrated or lagged response; rather than a direct, instantaneous record of dust-driven Hg delivery. Nonetheless, our evidence suggests that while dust fluxes to Ohrid clearly varied across glacial-interglacial periods, they were likely not a dominant factor in the observed Hg behavior.

Volcanic eruptions can also emit large quantities of Hg to the atmosphere (Pyle & Mather, 2003). Although the DEEP 5045-1 core contains multiple volcanic ash layers, clear evidence that volcanic ash clouds recurrently reached Lake Ohrid (Leicher et al., 2021), we find that individual ash layers in the DEEP 5045-1 core do not correspond to measurable peaks in $Hg_{T\text{-}CFB}$ or Hg_{AR}. This result is also consistent with published evidence from Lake Ohrid and neighboring Lake Prespa over the most recent ∼90 ka (Paine et al., 2024). Together, this evidence suggests either that fluxes of volcanic-sourced (atmospheric) Hg to the catchment of Lake Ohrid was not sufficiently high to leave a measurable signal in the sediments, and/or that our sample resolution was too coarse to identify single, short lived volcanogenic perturbations of the scale and type occurring during the period covered by DEEP 5045-1.

5.1.3. Modulation by Terrestrial Reservoirs

The lack of consistent glacial-interglacial cyclicity in the DEEP 5045-1 $Hg_{T\text{-}CFB}$ and Hg_{AR} curves (Figure 2) suggests that burial efficiency, not atmospheric flux changes, provide sufficient explanations for the variability that is observed in these Hg signals. Hence, we tested an alternative mechanism—flux modulation by local reservoirs (or "capacitors")—as potentially the most significant control on Hg variability in this system (Figure 3). Lake Ohrid is located in the mid-latitudes where terrestrial soil and forest reservoirs can (strongly) vary in size, meaning their influence on local Hg cycling are likely to be pronounced; specifically by holding significant amounts of Hg for relatively long periods ($>10^3$ years; Gustin et al., 2020). Ecosystems in this region are already known to be highly responsive to orbital-scale climate change (Donders et al., 2021), and recent studies have shown that vegetation and soils can serve as effective modulators of Hg cycling on decadal-to-centennial timescales (Jiskra et al., 2018; Zhou et al., 2021). From this, we propose that on glacial-interglacial timescales, regulation of local Hg supply to Lake Ohrid could be related to changes in hydrology, and reservoir stability (Wang et al., 2020).

Supply of Hg to Lake Ohrid appears to have been amplified when the catchment was marked by reductions in vegetation density, and biodiversity (Figures 5a–5e). e.g., intervals marked by low arboreal pollen (e.g., *AP-Pinus*), and elevated detrital material (e.g., quartz) concentrations have been interpreted in this record as signs of limited vegetation growth, pedogenesis (Ti/K), and soil stabilization by plant roots (Donders et al., 2021; Wagner et al., 2019). All would combine to enable more effective erosion and removal of soil materials by wind, rain, and periglacial processes, with rivers effectively transporting these eroded materials into the lake when the landscape was less covered by vegetation (Francke et al., 2016, 2019). Fine-grained detrital materials are also known to provide effective vectors for Hg delivery to lake basins (Nagorski et al., 2021; Staniszewska et al., 2023), and recent studies have shown that terrestrial Hg fluxes can increase in response to deforestation, reduced organic matter cycling (e.g., by litterfall), and soil destabilization (Wang et al., 2019): owing to increased erosion of soil matrices, and long-term reductions in the stability of terrestrial reservoirs (Gworek et al., 2020; Wang et al., 2020). This also implies that terrestrial biomass accumulation and development of thick soils would have the opposite effect: limiting mobilization of Hg by aeolian, hydrological, and cryospheric forces (Bishop et al., 2020). Our data on the variance in Hg and notably the evolution of cyclic behavior may suggest an important role for this mechanism, as lower $Hg_{T\text{-}CFB}$ and Hg_{AR} values indicative of reduced Hg export to the lake typically occur in conjunction with higher arboreal pollen percentages (Figure 5b), enhanced pedogenesis (Figure 5c), and higher local temperatures (Figure 3f): all indicative of a more "closed" catchment more susceptible to erosion, or mobilization, of Hg.

Climate-driven shifts in catchment structure also correspond to changes in regional hydrology. Lake Ohrid is hydrologically well connected to its catchment with continuous flow of water into the basin facilitated by karst springs and local river channels (Matzinger et al., 2006), and it is likely that ice caps were established in the mountains surrounding Lake Ohrid during glacial intervals (e.g., Gromig et al., 2018; Ruszkiczay-Rüdiger et al., 2020). Regional ice expansions on glacial-interglacial timescales can cause substantial changes in sediment supply to lakes, owing to processes such as de-buttressing, cryoturbation, freeze-thaw, and quarrying of fine-grained tills and sediments (e.g., Rodbell et al., 2022). All are processes known to influence Hg transport (Nagorski et al., 2021; Staniszewska et al., 2023), and so suggest that glacial expansion would have had important

implications for Hg cycling. For example, more intense erosion of organic and particulate-bound Hg by meltwaters emerging from englacial, subglacial or supraglacial conduits could have enhanced the overall flux of Hg to the Ohrid basin; especially if local soils were already degraded by the climate-driven recession of regional forest structures.

We propose that during intervals marked by less vegetation cover, reduced biodiversity, and elevated soil denudation (Figures 5a–5e), the resulting decline in terrestrial reservoir size and stability would diminish how effectively they could buffer, filter, and/or store Hg prior to reaching Lake Ohrid. This loss in Hg storage capacity would limit the catchment's function as a buffer/filter of Hg fluxes to the lake, enabling a more direct source-to-sink transfer pathway, and reducing residence times in domains where Hg can be readily re-evaded to the atmosphere (e.g., soils and surface waters; Bishop et al., 2020; Gworek et al., 2020). Hence, the combined effect of this reduced storage, diminished filtering, and more efficient routing would be a net increase in supply of Hg to the lake (Figure 5a), accompanied by a suppression of longer-term (multi-millennial-scale) regular Hg variability that is primarily generated by internal catchment processes. Under these conditions, the behavior of Hg in the sediment record through time would instead reflect a progressively noisier, more direct imprint of external forcings, with secondary modulation by global-scale processes such as ice cover and dust flux.

5.2. Evolution of Mercury Behavior

Ecological (namely vegetation and soil), glaciological, and sedimentological processes are all known to be critical within the terrestrial Hg cycle on millennial timescales (Fadina et al., 2019; Paine et al., 2024; Wang et al., 2024). Our record documents a transition toward less periodic, increasingly high-amplitude, and more "noisy" $Hg_{T\text{-}CFB}$ and Hg_{AR} behavior at ∼780 ka (Figure 5a). This transition deviates from key ecological proxies in the DEEP 5045-1 sediments, which instead document a clear shift from ∼41-kyr to high-amplitude ∼100-kyr cyclicity (Figures 5b and 5c; e.g., Donders et al., 2021; Wagner et al., 2019, 2022). Also evident from ∼780 ka is a reduction in the peak amplitude of arboreal pollen percentages (Figure 5b) and Ti/K ratios (Figure 5c), marking a progressive (net) reduction in local pedogenesis and arboreal pollen, respectively. Furthermore, examination of microfossil distributions throughout the DEEP 5045-1 core show that sedimentological shifts following the MPT were accompanied by increasing abundances of diatom taxa previously shown to coincide with large-scale changes in global ice volume and temperatures, such as *Pantocsekiella* (Cvetkoska et al., 2021; Wilke et al., 2020). Together, these sedimentological and biological proxies suggest that the Ohrid record does capture a distinct MPT-associated shift, and so the coeval timing of comparatively less periodic $Hg_{T\text{-}CFB}$ and Hg_{AR} behavior, decreasing vegetation diversity, tree cover, and soil stability could suggest that the sensitivity of Lake Ohrid's catchment to orbital-scale climate change had direct bearing on Hg supply and burial across the MPT.

Two ecological shifts across the MPT could provide a link between Hg oscillations in the DEEP 5045-1 record, and the orbital-scale evolution of Ohrid catchment. The first is a net reduction in local soil reservoir size and stability in response to longer glacial intervals, and their associated effects. Following the MPT and particularly since ∼400 ka, DEEP 5045-1 documents a progressive shift to the formation of thinner soil horizons, in the form of a clear reduction in the glacial-interglacial contrast between sedimentary Ti/K ratios (Figure 5c), suggesting that physical weathering became more important in the catchment relative to chemical weathering. Given that organic components that are chemically or physically mineral-bound can effectively stabilize Hg within the soil matrix, this suggests that soils would have stored not only less organic matter, but also less Hg (O'Connor et al., 2019; Wang et al., 2019).

An indirect control by soil carbon storage on Hg may seem counter to our identification of a negative correlation between Hg and TOC in Lake Ohrid (Figure 2, Figure S5 in Supporting Information S1) and the assessment from thermal desorption characteristics that Hg is likely associated with an organic phase. Indeed, it is important to note that measured sedimentary TOC is not equivalent to soil or terrestrial OM. Reduced primary productivity, and oxygenation of bottom waters (enhanced vertical mixing) would act to reduce TOC in the lake sediments during cooler glacial conditions, whereas the opposite occurs during warmer interglacials (Francke et al., 2016). Thus, during glacials, sedimentary TOC concentrations would fall while Hg inputs rose due to the increased soil denudation promoting Hg leaching into groundwater (Du et al., 2023), its greater transport via runoff (Bishop et al., 2020), and reduced Hg re-emission to the atmosphere as detailed above.

The second shift, which primarily affects above ground carbon and Hg reservoirs, is a decline in arboreal pollen and biodiversity, driven by more prolonged, eccentricity-paced climate cycles. This decline is documented in

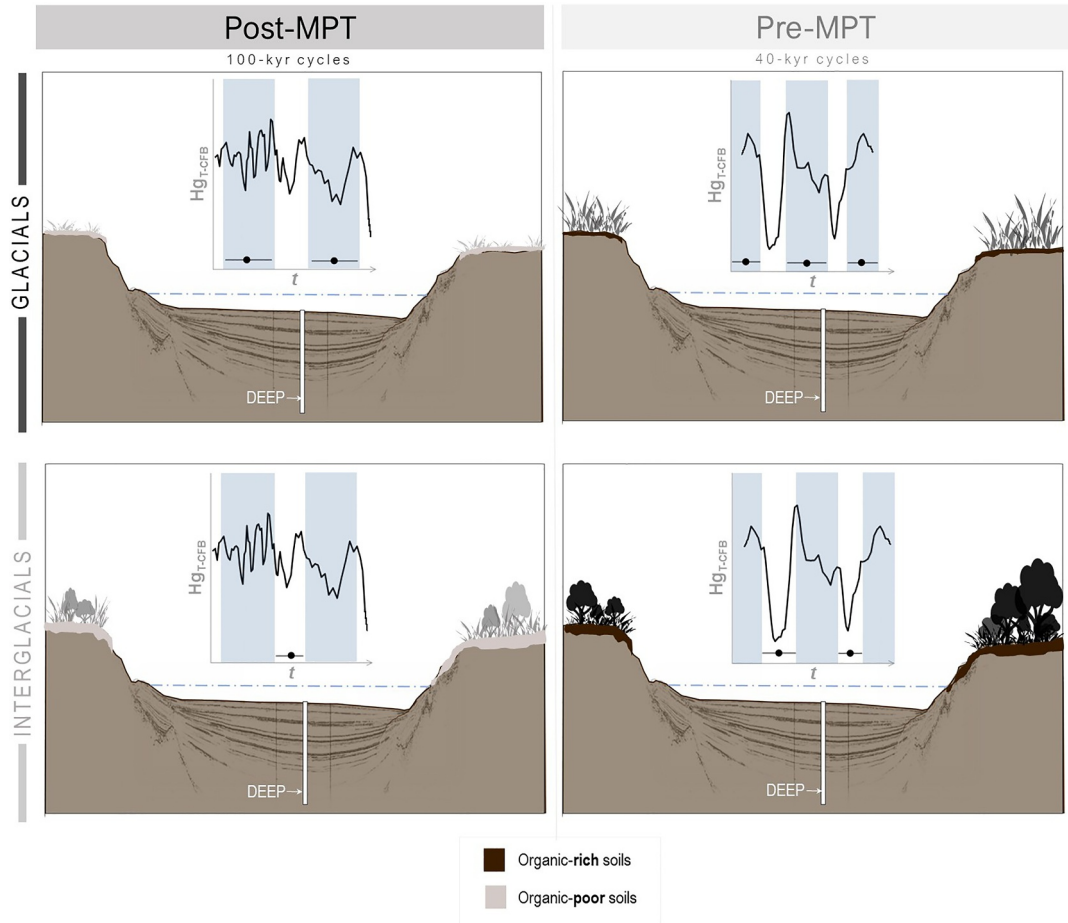

Figure 6. Schematic model depicting key changes in Hg supply to the sediments of Lake Ohrid prior to (~1,360–780 ka), and following (~780–0 ka) the Mid-Pleistocene transition (MPT). Diagrams are separated relative to glacial and interglacial intervals, where cartoon images show the contrast in vegetation and soil characteristics between each scenario (e.g., fewer tree icons in the post-MPT glacial panel depicts a more open, "steppe" catchment). (*Insets*) End-member time series that illustrate "typical" changes in sedimentary $Hg_{T\text{-}CFB}$ relative to glacial (blue shading) and interglacial conditions, and to each of the four states presented here. Shapes of these $Hg_{T\text{-}CFB}$ curves are derived from the data for MIS 38 to 32 (pre-MPT), and MIS 7 to 5c (post-MPT), presented in Figure 5.

Lake Ohrid as a progressive reduction in arboreal pollen percentages within the DEEP 5045-1 core (Figure 5b), and characterized more specifically by a clear reduction in deciduous and mesophyllous tree species during both glacial and interglacial intervals following the MPT (Donders et al., 2021). One direct consequence of this decline would be an overall reduction in the size and stability of the catchment's standing biomass reservoir. Ecosystems with low biodiversity are typically less able to "buffer" the negative effects of abrupt climate change, and so lack the stability necessary to provide effective storage reservoirs for carbon or Hg (Hararuk et al., 2013). When superimposed onto the MPT-induced prolongation of (cold) glacial cycles, it is possible that increasingly pronounced, orbital-scale ecological "swings" in the Ohrid catchment instigated a long-term decline in surface biomass (Figure 5b), reducing not only the overall capacity of vegetation to effectively uptake Hg (Zhou et al., 2021), but also destabilize their underlying soils, reduce litterfall Hg supplies, and concurrently reduce soil capacity for Hg storage (Wang et al., 2019; Yuan et al., 2024).

Taken together, we propose that the change in terrestrial Hg cycle behavior recorded by DEEP 5045-1 can be mechanistically explained by the mid-Pleistocene intensification of glacial cycles (Figure 6). Colder and more arid conditions would have suppressed pedogenesis and reduced net terrestrial primary productivity, limiting vegetation growth and the supply of organic matter that effectively binds and stabilizes Hg in soils (O'Connor et al., 2019). The reduced canopy cover would also limit direct Hg^0 uptake in leaves (Zhou et al., 2021), while

concurrent amplification of periglacial processes due to growth of glaciers and permafrost in the surrounding mountains would enhance Hg mobilization by ice and meltwaters (Nagorski et al., 2021; Staniszewska et al., 2023). Therefore, the enhanced amplitude of glacial–interglacial climate oscillations after the MPT could have induced two effects: (a) an overall reduction in Hg sequestration capacity in terrestrial reservoirs, and (b) an increase in the mobility of previously stored Hg. Resulting from this reduction in the effective Hg sink and thereby the modulatory capacity of terrestrial reservoirs would be a more direct pathway from atmospheric and detrital sources to lacustrine sinks.

5.3. Links to Terrestrial Carbon Reservoirs

An intriguing feature of the DEEP 5045-1 sedimentary record is the apparent decoupling of $Hg_{T\text{-}CFB}$ (local Hg cycle), TOC_{CFB}, and TIC (local carbon cycle) following the MPT. Prior to the MPT, coeval oscillations in $Hg_{T\text{-}CFB}$, TOC_{CFB}, and TIC correspond to periodic shifts in vegetation and soil cover, composition, and stability in the catchment (Figures 2 and 5). However, following establishment of ∼100-kyr glacial-interglacial cycles at ∼780 ka, TOC_{CFB} and TIC show increasingly pronounced contrasts between glacial and interglacial intervals, whereas the clear glacial-interglacial pattern in $Hg_{T\text{-}CFB}$ weakens significantly (Figure 4).

Recent studies have shown that the biological and physical processes that control the terrestrial organic carbon cycle also control the terrestrial Hg cycle (Yuan et al., 2024; Zhou et al., 2025). This coupling exists primarily as land-atmosphere exchanges of Hg and carbon are both modulated by uptake from the atmosphere in vegetation, storage and release through decomposition and combustion. All these factors are responsive to climate (Hararuk et al., 2013; Schaefer et al., 2020), and the close coupling between Hg uptake in vegetation and common Hg-organic-carbon association in soils imply that climate-driven terrestrial carbon reservoir dynamics could have also “echoed” effects in Hg reservoir dynamics. For example, both Hg and organic carbon fluxes to Lake Ohrid could have been affected by intensifying exposure and reworking of older (previously undisturbed) soils and sediments by physical erosion of surface soils and/or by meltwater discharges during glacials. However, it is not guaranteed that this correspondence would translate to coupled sedimentary signals, and indeed the same mechanisms underpinning a carbon-Hg cycle coupling in the Ohrid catchment could also explain why their associated proxies seemingly deviate in the post-MPT sections of the DEEP 5045-1 record. For example, as glacials became longer and more intense, organic carbon may be released as CO_2 in response to changing environmental conditions (Hararuk et al., 2013). Whereas, Hg release could occur due to both evaporation from the soil surface, and erosion of organic and inorganic soil constituents; increasing its mobility in the catchment (Fritsche et al., 2008). Thus, the partial decoupling of sedimentary signals aassociated with Hg and carbon cycling in DEEP 5045-1 may reflect differing sensitivities of these two cycles to glacial intensification; despite sharing several common transport pathways, and post-depositional processes (Zhou et al., 2025).

Considering the evidence currently available, the dissociation of terrestrial Hg and carbon cycling in Lake Ohrid following the MPT suggests that modulation of Hg deposition by terrestrial capacitors may have been a key factor of Hg variability in some intervals such as the (pre-) MPT interval, with other environmental factors also contributing to the regularity of the observed variations (Sections 5.1.1 and 5.1.2). Given the links known to exist between the terrestrial Hg and C cycles (Hararuk et al., 2013; Yuan et al., 2024; Zhou et al., 2025), we hypothesize that terrestrial Hg stocks over geological timescales may be responsive to changes in terrestrial carbon stocks and, therefore, that both local and global-scale variations in terrestrial C reservoirs can impact Hg records. This may have occurred during large (periodic) changes in terrestrial ecosystems such as recorded in Ohrid across multiple Pleistocene glacial-interglacial periods (Figures 5 and 6). Ecological shifts of this nature, therefore, warrant consideration in studies that aim to resolve Hg cycle variations from terrestrial archives directly, or cover periods of abrupt major vegetation and/or soil disturbance deeper in Earth's geological past (Dal Corso et al., 2020).

6. Conclusions

The ∼1,360-kyr sedimentary archive of Lake Ohrid is one of the longest continuous records of terrestrial Hg cycling currently available. The temporal scope of the sequence offers a unique opportunity to test the extent to which Hg responds over multiple glacial-interglacial cycles to environmental changes and which key processes may impact terrestrial Hg cycle behavior. Prior to ∼780 ka, total Hg concentrations corrected for carbonate dilution ($Hg_{T\text{-}CFB}$) and Hg accumulation rates (Hg_{AR}) both show significant orbital-scale cyclicity characterized by a ∼44-kyr (obliquity) component, with higher values typically corresponding to glacial intervals. Similarly

pronounced alterations to the terrestrial Hg cycle under glacial conditions have also been identified in records corresponding to the last glacial period (<100 ka; Paine et al., 2024, 2025; Schneider et al., 2020; Wang et al., 2024). However, very few terrestrial records exist that cover multiple glacial cycles. The DEEP 5045-1 Hg and paleoenvironmental record covers multiple glacial cycles, and synthesizing these data sets allows us to propose that the observed, pre-MPT $Hg_{T\text{-}CFB}$ variability could be explained by the sensitivity of vegetation and soils in the Ohrid catchment to climate, combined with the open hydrology of the lake.

After ~780 ka, there is a reduction in glacial-interglacial contrast between $Hg_{T\text{-}CFB}$ values, and peaks become increasingly higher in amplitude. This shift appears to diverge from other ecological proxies in the DEEP 5045-1 core, that show a clear shift from ~41-kyr to ~100-kyr cycles. From these observations, we suggest that the change in Hg response corresponds to a reduction in local soil formation and arboreal pollen in response to the mid-Pleistocene intensification of glacial cycles: with increasingly pronounced, orbital-scale ecological "swings" in the Ohrid catchment not only reducing the capacity for vegetation to effectively uptake Hg, but also destabilizing their underlying soils, reducing litterfall Hg supplies, and concurrently limiting the soil's capacity for Hg assimilation. Hence, our data suggest that orbital-scale environmental changes were important drivers of Hg cycle variability over many of the earlier >20 glacial-interglacial cycles recorded in this archive, but fewer of the later. The climate-sensitive nature of the proposed modulating reservoir (vegetation, soils) implies the Hg cycle behavior documented here should be widely considered in the interpretation of the Pleistocene glacial-interglacial Hg record as well as periods of significant terrestrial disturbances in the geological rock record.

Human-driven environmental pollution has made it more difficult to isolate (and thus understand) the natural Hg cycle variability recorded in modern lake sediments. In light of the signals captured by the Lake Ohrid sedimentary record, we suggest that development of similarly long, millennial-scale terrestrial sediment records could provide opportunities to establish a pre-industrial Hg cycle baseline over an extended timeframe, and so provide crucial context for understanding which mechanisms are most significant for transport, accumulation, and cycling of Hg in different environments, over multiple millennia. On an even broader scale, records of this nature could allow for closer study of Hg-cycle responses to other key climate transitions of the Quaternary, such as intensification of Northern Hemisphere Glaciation (INHG), intensification of the tropical Walker Circulation, and the older Heinrich events and Dansgaard-Oeschger (D-O) cycles. Comparison of Hg signals corresponding to intervals in which environmental conditions and/or responses to orbital cycles were distinctly different (e.g., pre-vs. post-MPT) could, therefore, allow for better differentiation of signals produced by the host system itself, and those produced by these external processes.

Conflict of Interest

The authors declare no conflicts of interest relevant to this study.

Availability Statement

Data for core DEEP 5045-1 generated as part of this study are archived within the PANGAEA online repository (Paine et al., 2026) (CC-BY-4.0; https://doi.org/10.1594/PANGAEA.993441). Secondary and/or pre-existing data from DEEP 5045-1 used in this study are available as in Supporting Information S1 data sets accompanying the publications of Wagner et al. (2019), Francke et al. (2016), Donders et al. (2021), and Wagner et al. (2022). Material from core DEEP 5045-1 is stored partly at the University of Cologne and at the MARUM core repository in Bremen, Germany, and is available on request.

Acknowledgments
ARP, JF, and TAM acknowledge funding from the European Research Council Consolidator Grant V-ECHO (ERC-2018-COG-8187 17-V-ECHO). ARP thanks David Thomas and Mona Edwards (School of Geography, Oxford) for logistical assistance with sample transfer and storage. ARP also thanks Matthew Jones and Victoria Smith for their insights and feedback during manuscript preparation. All authors thank two anonymous reviewers for their feedback, which further helped to improve the manuscript, and members of the Scientific Collaboration on Past Speciation Conditions in Lake Ohrid (SCOPSCO) for their efforts in producing the Lake Ohrid sediment successions and making the data available for scientific use. Open access publishing facilitated by Universitat Basel, as part of the Wiley - Universitat Basel agreement via the Consortium Of Swiss Academic Libraries.

References

Amos, H. M., Jacob, D. J., Kocman, D., Horowitz, H. M., Zhang, Y., Dutkiewicz, S., et al. (2014). Global biogeochemical implications of Mercury discharges from Rivers and sediment burial. *Environmental Science and Technology*, *48*(16), 9514–9522. https://doi.org/10.1021/es502134t

Bereiter, B., Eggleston, S., Schmitt, J., Nehrbass-Ahles, C., Stocker, T. F., Fischer, H., et al. (2015). Revision of the EPICA Dome C CO_2 record from 800 to 600-kyr before present. *Geophysical Research Letters*, *42*(2), 542–549. https://doi.org/10.1002/2014GL061957

Bin, C., Xiaoru, W., & Lee, F. S. C. (2001). Pyrolysis coupled with atomic absorption spectrometry for the determination of mercury in Chinese medicinal materials. *Analytica Chimica Acta*, *447*(1–2), 161–169. https://doi.org/10.1016/S0003-2670(01)01218-1

Bishop, K., Shanley, J. B., Riscassi, A., de Wit, H. A., Eklöf, K., Meng, B., et al. (2020). Recent advances in understanding and measurement of mercury in the environment: Terrestrial Hg cycling. *Science of the Total Environment*, *721*, 137647. https://doi.org/10.1016/j.scitotenv.2020.137647

Bravo, A. G., Bouchet, S., Tolu, J., Björn, E., Mateos-Rivera, A., & Bertilsson, S. (2017). Molecular composition of organic matter controls methylmercury formation in boreal lakes. *Nature Communications*, *8*(1), 14255. https://doi.org/10.1038/ncomms14255

Chede, B. S., Venancio, I. M., Figueiredo, T. S., Albuquerque, A. L. S., & Silva-Filho, E. V. (2022). Mercury deposition in the western tropical South Atlantic during the last 70 ka. *Palaeogeography, Palaeoclimatology, Palaeoecology*, *601*, 111122. https://doi.org/10.1016/j.palaeo.2022.111122

Clark, P. U., Archer, D., Pollard, D., Blum, J. D., Rial, J. A., Brovkin, V., et al. (2006). The middle Pleistocene transition: Characteristics, mechanisms, and implications for long-term changes in atmospheric pCO2. *Quaternary Science Reviews*, *25*(23–24), 3150–3184. https://doi.org/10.1016/j.quascirev.2006.07.008

Clarke, R. G., Klapstein, S. J., Keenan, R., & O'Driscoll, N. J. (2023). Mercury photoreduction and photooxidation kinetics in estuarine water: Effects of salinity and dissolved organic matter. *Chemosphere*, *312*, 137279. https://doi.org/10.1016/j.chemosphere.2022.137279

Cvetkoska, A., Jovanovska, E., Hauffe, T., Donders, T. H., Levkov, Z., Van De Waal, D. B., et al. (2021). Drivers of phytoplankton community structure change with ecosystem ontogeny during the Quaternary. *Quaternary Science Reviews*, *265*, 107046. https://doi.org/10.1016/j.quascirev.2021.107046

Dal Corso, J., Mills, B. J. W., Chu, D., Newton, R. J., Mather, T. A., Shu, W., et al. (2020). Permo–Triassic boundary carbon and mercury cycling linked to terrestrial ecosystem collapse. *Nature Communications*, *11*, 1–9. https://doi.org/10.1038/s41467-020-16725-4

Donders, T., Panagiotopoulos, K., Koutsodendris, A., Bertini, A., Mercuri, A. M., Masi, A., et al. (2021). 1.36 million years of Mediterranean forest Refugium dynamics in response to glacial-interglacial cycle strength. *Proceedings of the National Academy of Sciences of the United States of America*, *118*(34), e2026111118. https://doi.org/10.1073/pnas.2026111118

Du, H., Wang, X., Yuan, W., Wu, F., Jia, L., Liu, N., et al. (2023). Elevated Mercury deposition, accumulation, and migration in a karst Forest. *Environmental Science and Technology*, *57*(45), 17490–17500. https://doi.org/10.1021/acs.est.3c05409

Fadina, O. A., Venancio, I. M., Belem, A., Silveira, C. S., Bertagnolli, D. C., Silva-Filho, E. V., & Albuquerque, A. L. S. (2019). Paleoclimatic controls on mercury deposition in northeast Brazil since the Last Interglacial. *Quaternary Science Reviews*, *221*, 105869. https://doi.org/10.1016/j.quascirev.2019.105869

Fendley, I. M., Frieling, J., Mather, T. A., Ruhl, M., Hesselbo, S. P., & Jenkyns, H. C. (2024). Early Jurassic large igneous province carbon emissions constrained by sedimentary mercury. *Nature Geoscience*, *17*(3), 241–248. https://doi.org/10.1038/s41561-024-01378-5

Figueiredo, T. S., Bergquist, B. A., Santos, T. P., Albuquerque, A. L. S., & Silva-Filho, E. V. (2022). Relationship between glacial CO_2 drawdown and mercury cycling in the western South Atlantic: An isotopic insight. *Geology*, *50*, 3–7. https://doi.org/10.1130/g49942.1

Filippelli, G. M. (2008). The global phosphorus cycle: Past, present, and future. *Elements*, *4*, 89–95. https://doi.org/10.2113/GSELEMENTS.4.2.89

Francke, A., Dosseto, A., Panagiotopoulos, K., Leicher, N., Lacey, J. H., Kyrikou, S., et al. (2019). Sediment residence time reveals Holocene shift from climatic to vegetation control on catchment erosion in the Balkans. *Global and Planetary Change*, *177*, 186–200. https://doi.org/10.1016/j.gloplacha.2019.04.005

Francke, A., Wagner, B., Just, J., Leicher, N., Gromig, R., Baumgarten, H., et al. (2016). Sedimentological processes and environmental variability at Lake Ohrid (Macedonia, Albania) between 637 ka and the present. *Biogeosciences*, *13*(4), 1179–1196. https://doi.org/10.5194/bg-13-1179-2016

Frieling, J., Fendley, I. M., Nawaz, M. A., & Mather, T. A. (2024). Assessment of Hg speciation changes in the sedimentary rock record from thermal desorption characteristics. *Geochemistry, Geophysics, Geosystems*, *25*(4), e2024GC011502. https://doi.org/10.1029/2024GC011502

Frieling, J., Mather, T. A., Fendley, I. M., Jenkyns, H. C., Zhao, Z., Dahl, T. W., et al. (2024). No evidence for a volcanic trigger for late Cambrian carbon-cycle perturbations. *Geology*, *52*(1), 12–16. https://doi.org/10.1130/G51570.1

Frieling, J., Mather, T. A., März, C., Jenkyns, H. C., Hennekam, R., Reichart, G.-J., et al. (2023). Effects of redox variability and early diagenesis on marine sedimentary Hg records. *Geochimica et Cosmochimica Acta*, *351*, 78–95. https://doi.org/10.1016/j.gca.2023.04.015

Fritsche, J., Obrist, D., Zeeman, M., Conen, F., Eugster, W., & Alewell, C. (2008). Elemental mercury fluxes over a sub-alpine grassland determined with two micrometeorological methods. *Atmospheric Environment*, *42*(13), 2922–2933. https://doi.org/10.1016/j.atmosenv.2007.12.055

Gagnon, C., Pelletier, É., & Mucci, A. (1997). Behaviour of anthropogenic mercury in coastal marine sediments. *Marine Chemistry*, *59*(1–2), 159–176. https://doi.org/10.1016/S0304-4203(97)00071-6

Grant, K. M., Rohling, E. J., Westerhold, T., Zabel, M., Heslop, D., Konijnendijk, T., & Lourens, L. (2017). A 3 million year index for North African humidity/aridity and the implication of potential Pan-African Humid periods. *Quaternary Science Reviews*, *171*, 100–118. https://doi.org/10.1016/j.quascirev.2017.07.005

Gromig, R., Mechernich, S., Ribolini, A., Wagner, B., Zanchetta, G., Isola, I., et al. (2018). Evidence for a Younger Dryas deglaciation in the Galicica Mountains (FYROM) from cosmogenic 36Cl. *Quaternary International*, *464*, 352–363. https://doi.org/10.1016/j.quaint.2017.07.013

Gustin, M. S., Bank, M. S., Bishop, K., Bowman, K., Branfireun, B., Chételat, J., et al. (2020). Mercury biogeochemical cycling: A synthesis of recent scientific advances. *The Science of the Total Environment*, *737*, 139619. https://doi.org/10.1016/j.scitotenv.2020.139619

Gworek, B., Dmuchowski, W., & Baczewska-Dąbrowska, A. H. (2020). Mercury in the terrestrial environment: A review. *Environmental Sciences Europe*, *32*(1), 128. https://doi.org/10.1186/s12302-020-00401-x

Hammer, Ø., Harper, D. A. T., & Ryan, P. D. (2001). PAST: Paleontological statistics software package for education and data analysis. *Palaeontologia Electronica*, *4*, 9.

Hararuk, O., Obrist, D., & Luo, Y. (2013). Modelling the sensitivity of soil mercury storage to climate-induced changes in soil carbon pools. *Biogeosciences*, *10*(4), 2393–2407. https://doi.org/10.5194/bg-10-2393-2013

Hoffmann, N., Reicherter, K., Fernández-Steeger, T., & Grützner, C. (2010). Evolution of ancient Lake Ohrid: A tectonic perspective. *Biogeosciences*, *7*(10), 3377–3386. https://doi.org/10.5194/bg-7-3377-2010

Huang, J., Kang, S., Yin, R., Ram, K., Liu, X., Lu, H., et al. (2020). Desert dust as a significant carrier of atmospheric mercury. *Environmental Pollution*, *267*, 115442. https://doi.org/10.1016/j.envpol.2020.115442

Jiskra, M., Sonke, J. E., Obrist, D., Bieser, J., Ebinghaus, R., Myhre, C. L., et al. (2018). A vegetation control on seasonal variations in global atmospheric mercury concentrations. *Nature Geoscience*, *11*(4), 244–250. https://doi.org/10.1038/s41561-018-0078-8

Kovács, E. B., Ruhl, M., Silva, R. L., McElwain, J. C., Reolid, M., Korte, C., et al. (2024). Mercury sequestration pathways under varying depositional conditions during early Jurassic (Pliensbachian and Toarcian) Karoo-Ferrar volcanism. *Palaeogeography, Palaeoclimatology, Palaeoecology*, *637*, 111977. https://doi.org/10.1016/j.palaeo.2023.111977

Lacey, J. H., Leng, M. J., Francke, A., Sloane, H. H., Milodowski, A., Vogel, H., et al. (2016). Northern Mediterranean climate since the Middle Pleistocene: A 637 ka stable isotope record from Lake Ohrid (Albania/Macedonia). *Biogeosciences*, *13*(6), 1801–1820. https://doi.org/10.5194/bg-13-1801-2016

Laskar, J., Robutel, P., Joutel, F., Gastineau, M., Correia, A. C. M., & Levrard, B. (2004). A long-term numerical solution for the insolation quantities of the Earth. *Astronomy and Astrophysics*, *428*(1), 261–285. https://doi.org/10.1051/0004-6361:20041335

Leicher, N., Giaccio, B., Zanchetta, G., Sulpizio, R., Albert, P. G., Tomlinson, E. L., et al. (2021). Lake Ohrid's tephrochronological dataset reveals 1.36 Ma of Mediterranean explosive volcanic activity. *Scientific Data*, *8*, 1–14. https://doi.org/10.1038/s41597-021-01013-7

Lisiecki, L. E., & Raymo, M. E. (2005). A Pliocene-Pleistocene stack of 57 globally distributed benthic $\delta^{18}O$ records. *Paleoceanography*, *20*, 1–17. https://doi.org/10.1029/2004PA001071

Matzinger, A., Jordanoski, M., Veljanoska-Sarafiloska, E., Sturm, M., Müller, B., & Wüest, A. (2006). Is Lake Prespa jeopardizing the ecosystem of ancient Lake Ohrid? *Hydrobiologia*, *553*(1), 89–109. https://doi.org/10.1007/s10750-005-6427-9

Meyers, S. R. (2014). Astrochron: An R package for astrochronology.

Nagorski, S. A., Vermilyea, A. W., & Lamborg, C. H. (2021). Mercury export from glacierized Alaskan watersheds as influenced by bedrock geology, watershed processes, and atmospheric deposition. *Geochimica et Cosmochimica Acta*, *304*, 32–49. https://doi.org/10.1016/j.gca.2021.04.003

Obrist, D., Kirk, J. L., Zhang, L., Sunderland, E. M., Jiskra, M., & Selin, N. E. (2018). A review of global environmental mercury processes in response to human and natural perturbations: Changes of emissions, climate, and land use. *Ambio*, *47*(2), 116–140. https://doi.org/10.1007/s13280-017-1004-9

O'Connor, D., Hou, D., Ok, Y. S., Mulder, J., Duan, L., Wu, Q., et al. (2019). Mercury speciation, transformation, and transportation in soils, atmospheric flux, and implications for risk management: A critical review. *Environment International*, *126*, 747–761. https://doi.org/10.1016/j.envint.2019.03.019

O'Driscoll, N. J., Vost, E., Mann, E., Klapstein, S., Tordon, R., & Lukeman, M. (2018). Mercury photoreduction and photooxidation in lakes: Effects of filtration and dissolved organic carbon concentration. *Journal of Environmental Sciences*, *68*, 151–159. https://doi.org/10.1016/j.jes.2017.12.010

Outridge, P. M., Mason, R. P., Wang, F., Guerrero, S., & Heimbürger-Boavida, L. E. (2018). Updated global and Oceanic Mercury budgets for the united Nations global Mercury assessment 2018. *Environmental Science and Technology*, *52*, 11466–11477. https://doi.org/10.1021/acs.est.8b01246

Paine, A. R., Fendley, I. M., Frieling, J., Mather, T. A., Lacey, J. H., Wagner, B., et al. (2024). Mercury records covering the past 90 000 years from lakes Prespa and Ohrid, SE Europe. *Biogeosciences*, *21*(2), 531–556. https://doi.org/10.5194/bg-21-531-2024

Paine, A. R., Frieling, J., Shanahan, T. M., Mather, T. A., McKay, N., Robinson, S. A., et al. (2025). Evidence for millennial-scale interactions between Hg cycling and hydroclimate from Lake Bosumtwi, Ghana. *Climate of the Past*, *21*(4), 817–839. https://doi.org/10.5194/cp-21-817-2025

Paine, A. R., Frieling, J., Wagner, B., Francke, A., Lacey, J. H., Mather, T. A., et al. (2026). Sedimentary mercury measurements for core ICDP DEEP 5045-1, Lake Ohrid [Dataset]. https://doi.org/10.1594/PANGAEA.993441

Palacios, D., Hughes, P. D., García-Ruiz, J. M., & Andrés, N. (2022). The Quaternary ice ages. In *European glacial landscapes* (pp. 9–18). Elsevier. https://doi.org/10.1016/B978-0-12-823498-3.00006-6

Pérez-Rodríguez, M., Margalef, O., Corella, J. P., Saiz-Lopez, A., Pla-Rabes, S., Giralt, S., & Cortizas, A. M. (2018). The role of climate: 71 ka of atmospheric mercury deposition in the southern hemisphere recorded by Rano Aroi Mire, Easter Island (Chile). *Geosciences*, *8*(10), 374. https://doi.org/10.3390/geosciences8100374

Pyle, D. M., & Mather, T. A. (2003). The importance of volcanic emissions for the global atmospheric mercury cycle. *Atmospheric Environment*, *37*(36), 5115–5124. https://doi.org/10.1016/j.atmosenv.2003.07.011

Qin, X., Guo, Q., Martens, P., & Krafft, T. (2024). Mercury stable isotopes revealing the atmospheric mercury circulation: A review of particulate bound mercury in China. *Earth-Science Reviews*, *250*, 104681. https://doi.org/10.1016/j.earscirev.2024.104681

Ren, H., Sigman, D. M., Martínez-García, A., Anderson, R. F., Chen, M.-T., Ravelo, A. C., et al. (2017). Impact of glacial/interglacial sea level change on the ocean nitrogen cycle. *Proceedings of the National Academy of Sciences of the United States of America*, *114*(33). https://doi.org/10.1073/pnas.1701315114

Rodbell, D. T., Hatfield, R. G., Abbott, M. B., Chen, C. Y., Woods, A., Stoner, J. S., et al. (2022). 700,000 years of tropical Andean glaciation. *Nature*, *607*(7918), 301–306. https://doi.org/10.1038/s41586-022-04873-0

Ruszkiczay-Rüdiger, Z., Kern, Z., Temovski, M., Madarász, B., Milevski, I., & Braucher, R. (2020). Last deglaciation in the central Balkan Peninsula: Geochronological evidence from the Jablanica mt. (North Macedonia). *Geomorphology*, *351*, 106985. https://doi.org/10.1016/j.geomorph.2019.106985

Sahoo, P. K., Guimarães, J. T. F., Salomão, G. N., Reis, L. S., Da Silva, E. F., De Figueiredo, M. M. J. C., et al. (2023). Historical Hg accumulation (~65 cal kyr BP) in upland lakes of the Southeastern Brazilian Amazonia: New evidence of the extent of geogenic and diagenetic control. *The Science of the Total Environment*, *912*, 168930. https://doi.org/10.1016/j.scitotenv.2023.168930

Saniewska, D., & Bełdowska, M. (2017). Mercury fractionation in soil and sediment samples using thermo-desorption method. *Talanta*, *168*, 152–161. https://doi.org/10.1016/j.talanta.2017.03.026

Schaefer, K., Elshorbany, Y., Jafarov, E., Schuster, P. F., Striegl, R. G., Wickland, K. P., & Sunderland, E. M. (2020). Potential impacts of mercury released from thawing permafrost. *Nature Communications*, *11*, 1–6. https://doi.org/10.1038/s41467-020-18398-5

Schneider, L., Cooke, C. A., Stansell, N. D., & Haberle, S. G. (2020). Effects of climate variability on mercury deposition during the Older Dryas and Younger Dryas in the Venezuelan Andes. *Journal of Paleolimnology*, *63*(3), 211–224. https://doi.org/10.1007/s10933-020-00111-7

Segato, D., Saiz-Lopez, A., Mahajan, A. S., Wang, F., Corella, J. P., Cuevas, C. A., et al. (2023). Arctic mercury flux increased through the Last Glacial Termination with a warming climate. *Nature Geoscience*, *16*(5), 439–445. https://doi.org/10.1038/s41561-023-01172-9

Selin, N. E. (2009). Global biogeochemical cycling of mercury: A review. *Annual Review of Environment and Resources*, *34*(1), 43–63. https://doi.org/10.1146/annurev.environ.051308.084314

Shen, J., Feng, Q., Algeo, T. J., Liu, J., Zhou, C., Wei, W., et al. (2020). Sedimentary host phases of mercury (Hg) and implications for use of Hg as a volcanic proxy. *Earth and Planetary Science Letters*, *543*, 116333. https://doi.org/10.1016/j.epsl.2020.116333

Staniszewska, K. J., Reyes, A. V., & Cooke, C. A. (2023). Glacial erosion drives high summer Mercury exports from the Yukon River, Canada. *Environmental Science and Technology Letters*, *10*(11), 1117–1124. https://doi.org/10.1021/acs.estlett.3c00427

Tzedakis, P. C., Hooghiemstra, H., & Pälike, H. (2006). The last 1.35 million years at Tenaghi Philippon: Revised chronostratigraphy and long-term vegetation trends. *Quaternary Science Reviews*, *25*(23–24), 3416–3430. https://doi.org/10.1016/j.quascirev.2006.09.002

Van Der Bolt, B., Van Nes, E. H., Bathiany, S., Vollebregt, M. E., & Scheffer, M. (2018). Climate reddening increases the chance of critical transitions. *Nature Climate Change*, *8*(6), 478–484. https://doi.org/10.1038/s41558-018-0160-7

Vogel, H., Wagner, B., Zanchetta, G., Sulpizio, R., & Rosén, P. (2010). A paleoclimate record with tephrochronological age control for the last glacial-interglacial cycle from Lake Ohrid, Albania and Macedonia. *Journal of Paleolimnology*, *44*(1), 295–310. https://doi.org/10.1007/s10933-009-9404-x

Wagner, B., Tauber, P., Francke, A., Leicher, N., Binnie, S. A., Cvetkoska, A., et al. (2022). The geodynamic and limnological evolution of Balkan Lake Ohrid, possibly the oldest extant lake in Europe. *Boreas bor*, *12601*(1), 1–26. https://doi.org/10.1111/bor.12601

Wagner, B., Vogel, H., Francke, A., Friedrich, T., Donders, T., Lacey, J. H., et al. (2019). Mediterranean winter rainfall in phase with African monsoons during the past 1.36 million years. *Nature*, *573*(7773), 256–260. https://doi.org/10.1038/s41586-019-1529-0

Wang, X., Luo, J., Yuan, W., Lin, C. J., Wang, F., Liu, C., et al. (2020). Global warming accelerates uptake of atmospheric mercury in regions experiencing glacier retreat. *Proceedings of the National Academy of Sciences of the United States of America*, *117*(4), 2049–2055. https://doi.org/10.1073/pnas.1906930117

Wang, X., Yuan, W., Lin, C.-J., Zhang, L., Zhang, H., & Feng, X. (2019). Climate and vegetation as primary drivers for global Mercury storage in surface soil. *Environmental Science and Technology*, *53*(18), 10665–10675. https://doi.org/10.1021/acs.est.9b02386

Wang, X., Zhong, W., Quan, M., Li, T., Lin, D., & Zhang, C. (2024). Asynchronous variations of mercury accumulation since the last deglaciation in the eastern and western Nanling mountains in South China. *Quaternary Science Reviews*, *325*, 108490. https://doi.org/10.1016/j.quascirev.2023.108490

Wilke, T., Hauffe, T., Jovanovska, E., Cvetkoska, A., Donders, T., Ekschmitt, K., et al. (2020). Deep drilling reveals massive shifts in evolutionary dynamics after formation of ancient ecosystem. *Science Advances*, *6*(40), eabb2943. https://doi.org/10.1126/sciadv.abb2943

Xue, W., Xu, Z., Cheng, X., Gou, L., He, M., Jin, Z., et al. (2025). Glacial-Interglacial climate cycles of atmospheric Hg deposition: Insights from Hg isotopes in loess-paleosol sequences on the Chinese Loess Plateau. *Geophysical Research Letters*, *52*(7), e2024GL113960. https://doi.org/10.1029/2024GL113960

Yamamoto, M., Clemens, S. C., Seki, O., Tsuchiya, Y., Huang, Y., O'ishi, R., & Abe-Ouchi, A. (2022). Increased interglacial atmospheric CO_2 levels followed the mid-pleistocene transition. *Nature Geoscience*, *15*(4), 307–313. https://doi.org/10.1038/s41561-022-00918-1

Yu, J., Anderson, R. F., Jin, Z. D., Ji, X., Thornalley, D. J. R., Wu, L., et al. (2023). Millennial atmospheric CO_2 changes linked to ocean ventilation modes over past 150,000 years. *Nature Geoscience*, *16*(12), 1166–1173. https://doi.org/10.1038/s41561-023-01297-x

Yuan, T., Huang, S., Zhang, P., Song, Z., Ge, J., Miao, X., et al. (2024). Potential decoupling of CO_2 and Hg uptake process by global vegetation in the 21st century. *Nature Communications*, *15*(1), 4490. https://doi.org/10.1038/s41467-024-48849-2

Zhou, C., Liu, M., Mason, R. P., Assavapanuvat, P., Zhang, N. H., Bianchi, T. S., et al. (2025). Warming-induced retreat of West Antarctic glaciers weakened carbon sequestration ability but increased mercury enrichment. *Nature Communications*, *16*(1), 1831. https://doi.org/10.1038/s41467-025-57085-1

Zhou, J., Obrist, D., Dastoor, A., Jiskra, M., & Ryjkov, A. (2021). Vegetation uptake of mercury and impacts on global cycling. *Nature Reviews Earth & Environment*, *2*(4), 269–284. https://doi.org/10.1038/s43017-021-00146-y

References From the Supporting Information

Bar-Matthews, M., Ayalon, A., Gilmour, M., Matthews, A., & Hawkesworth, C. J. (2003). Sea - Land oxygen isotopic relationships from planktonic Foraminifera and speleothems in the Eastern Mediterranean region and their implication for paleorainfall during interglacial intervals. *Geochimica et Cosmochimica Acta*, *67*(17), 3181–3199. https://doi.org/10.1016/S0016-7037(02)01031-1

Bełdowska, M., Saniewska, D., Gębka, K., Kwasigroch, U., Korejwo, E., & Kobos, J. (2018). Simple screening technique for determination of adsorbed and absorbed mercury in particulate matter in atmospheric and aquatic environment. *Talanta*, *182*, 340–347. https://doi.org/10.1016/j.talanta.2018.01.082

Biester, H., & Scholz, C. (1997). Determination of Mercury binding forms in contaminated soils: Mercury pyrolysis versus sequential extractions. *Environmental Science and Technology*, *31*(1), 233–239. https://doi.org/10.1021/es960369h

Bombach, G., Bombach, K., & Klemm, W. (1994). Speciation of mercury in soils and sediments by thermal evaporation and cold vapor atomic absorption. *Fresenius' Journal of Analytical Chemistry*, *350*(1–2), 18–20. https://doi.org/10.1007/BF00326246

Gallagher, K., Bodin, T., Sambridge, M., Weiss, D., Kylander, M., & Large, D. (2011). Inference of abrupt changes in noisy geochemical records using transdimensional changepoint models. *Earth and Planetary Science Letters*, *311*(1–2), 182–194. https://doi.org/10.1016/j.epsl.2011.09.015

Grasby, S. E., Them, T. R., Chen, Z., Yin, R., & Ardakani, O. H. (2019). Mercury as a proxy for volcanic emissions in the geologic record. *Earth-Science Reviews*, *196*, 102880. https://doi.org/10.1016/j.earscirev.2019.102880

Grygar, T. M., Mach, K., & Martinez, M. (2019). Checklist for the use of potassium concentrations in siliciclastic sediments as paleoenvironmental archives. *Sedimentary Geology*, *382*, 75–84. https://doi.org/10.1016/j.sedgeo.2019.01.010

Horvat, M., Jereb, V., Fajon, V., Logar, M., Kotnik, J., Faganeli, J., et al. (2002). Mercury distribution in water, sediment and soil in the Idrijca and Sočhca river systems. *Geochemistry: Exploration, Environment, Analysis*, *2*(3), 287–296. https://doi.org/10.1144/1467-787302-033

Jebrak, M., & Hernandez, A. (1995). Tectonic deposition of mercury in the Almaden district, Las Cuevas deposit, Spain. *Mineralium Deposita*, *30*, 413–423.

Lézine, A. M., von Grafenstein, U., Andersen, N., Belmecheri, S., Bordon, A., Caron, B., et al. (2010). Lake Ohrid, Albania, provides an exceptional multi-proxy record of environmental changes during the last glacial-interglacial cycle. *Palaeogeography, Palaeoclimatology, Palaeoecology*, *287*(1–4), 116–127. https://doi.org/10.1016/j.palaeo.2010.01.016

Lindhorst, K., Krastel, S., Reicherter, K., Stipp, M., Wagner, B., & Schwenk, T. (2015). Sedimentary and tectonic evolution of Lake Ohrid (Macedonia/Albania). *Basin Research*, *27*(1), 84–101. https://doi.org/10.1111/bre.12063

Matter, M., Anselmetti, F. S., Jordanoska, B., Wagner, B., Wessels, M., & Wüest, A. (2010). Carbonate sedimentation and effects of eutrophication observed at the Kališta subaquatic springs in Lake Ohrid (Macedonia). *Biogeosciences*, *7*(11), 3755–3767. https://doi.org/10.5194/bg-7-3755-2010

Melard, G. (1984). Algorithm AS 197: A fast algorithm for the exact likelihood of autoregressive-moving average models. *Applied Statistics*, *33*(1), 104. https://doi.org/10.2307/2347672

Nalbant, J., Schneider, L., Hamilton, R., Connor, S., Biester, H., Stuart-Williams, H., et al. (2023). Fire, volcanism and climate change: The main factors controlling mercury (Hg) accumulation rates in Tropical Lake Lantoa, Sulawesi, Indonesia (~16,500–540 cal yr BP). *Front. Environ. Chem.*, *4*, 1241176. https://doi.org/10.3389/fenvc.2023.1241176

Nasr, M., & Arp, P. A. (2017). Mercury and organic matter concentrations in Lake and stream sediments in relation to one another and to atmospheric Mercury deposition and climate variations across Canada. *Journal of Chemistry*, *2017*, 1–21. https://doi.org/10.1155/2017/8949502

Niespolo, E. M., Rutte, D., Deino, A. L., & Renne, P. R. (2017). Intercalibration and Age of the Alder Creek sanidine $^{40}Ar/^{39}Ar$ standard. *Quaternary Geochronology*, *39*, 205–213. https://doi.org/10.1016/j.quageo.2016.09.004

Panagiotopoulos, K., Holtvoeth, J., Kouli, K., Marinova, E., Francke, A., Cvetkoska, A., et al. (2020). Insights into the evolution of the young Lake Ohrid ecosystem and vegetation succession from a southern European refugium during the early Pleistocene. *Quaternary Science Reviews*, *227*, 106044. https://doi.org/10.1016/j.quascirev.2019.106044

Petranich, E., Predonzani, S., Acquavita, A., Mashyanov, N., & Covelli, S. (2022). Applied Geochemistry Rapid thermoscanning technique for direct analysis of mercury species in contaminated sediments: From pure compounds to real sample application. *Applied Geochemistry*, *143*, 105393. https://doi.org/10.1016/j.apgeochem.2022.105393

Popovska, C., & Bonacci, O. (2007). Basic data on the hydrology of Lakes Ohrid and Prespa. *Hydrological Processes*, *21*(5), 658–664. https://doi.org/10.1002/hyp.6252

Renne, P. R., Balco, G., Ludwig, K. R., Mundil, R., & Min, K. (2011). Response to the comment by W.H. Schwarz et al. on "Joint determination of ^{40}K decay constants and ^{40}Ar*/^{40}K for the Fish Canyon sanidine standard, and improved accuracy for ^{40}Ar/39Ar geochronology" by P. R. Renne et al., *Geochimica et Cosmochimica Acta*, (Vol. 75(17), pp. 5097–5100). https://doi.org/10.1016/j.gca.2011.06.021

Rumayor, M., Diaz-Somoano, M., Lopez-Anton, M. A., & Martinez-Tarazona, M. R. (2013). Mercury compounds characterization by thermal desorption. *Talanta*, *114*, 318–322. https://doi.org/10.1016/j.talanta.2013.05.059

Rumayor, M., Lopez-Anton, M. A., Díaz-Somoano, M., & Martínez-Tarazona, M. R. (2015). A new approach to mercury speciation in solids using a thermal desorption technique. *Fuel*, *160*, 525–530. https://doi.org/10.1016/j.fuel.2015.08.028

Schulz, M., & Mudelsee, M. (2002). REDFIT: Estimating red-noise spectra directly from unevenly spaced paleoclimatic time series. *Computers and Geosciences*, *28*(3), 421–426. https://doi.org/10.1016/S0098-3004(01)00044-9

Schuster, P. F., Schaefer, K. M., Aiken, G. R., Antweiler, R. C., Dewild, J. F., Gryziec, J. D., et al. (2018). Permafrost stores a globally significant amount of Mercury. *Geophysical Research Letters*, *45*(3), 1463–1471. https://doi.org/10.1002/2017GL075571

Torrence, C., & Compo, G. P. (1998). A practical guide to wavelet analysis. *Bulletin America Meteorology Social*, *79*(1), 61–78. https://doi.org/10.1175/1520-0477(1998)079<0061:apgtwa>2.0.co;2

Trauth, M. H. (2021). Spectral analysis in Quaternary sciences. *Quaternary Science Reviews*, *270*, 107157. https://doi.org/10.1016/j.quascirev.2021.107157

Ulfers, A., Zeeden, C., Wagner, B., Krastel, S., Buness, H., & Wonik, T. (2022). Borehole logging and seismic data from Lake Ohrid (North Macedonia/Albania) as a basis for age-depth modelling over the last one million years. *Quaternary Science Reviews*, *276*, 107295. https://doi.org/10.1016/j.quascirev.2021.107295

VanderPlas, J. T. (2018). Understanding the lomb–scargle periodogram. *ApJS*, *236*(1), 16. https://doi.org/10.3847/1538-4365/aab766

Wagner, B., Wilke, T., Francke, A., Albrecht, C., Baumgarten, H., Bertini, A., et al. (2017). The environmental and evolutionary history of Lake Ohrid (FYROM/Albania): Interim results from the SCOPSCO deep drilling project. *Biogeosciences*, *14*(8), 2033–2054. https://doi.org/10.5194/bg-14-2033-2017

Wagner, B., Wilke, T., Krastel, S., Zanchetta, G., Sulpizio, R., Reicherter, K., et al. (2014). The SCOPSCO drilling project recovers more than 1.2 million years of history from Lake Ohrid. *Scientific Drilling*, *17*, 19–29. https://doi.org/10.5194/sd-17-19-2014

Warrier, A. K., Pednekar, H., Mahesh, B. S., Mohan, R., & Gazi, S. (2016). Sediment grain size and surface textural observations of quartz grains in late quaternary lacustrine sediments from Schirmacher Oasis, East Antarctica: Paleoenvironmental significance. *Polar Science*, *10*(1), 89–100. https://doi.org/10.1016/j.polar.2015.12.005

Wennrich, V., Francke, A., Dehnert, A., Juschus, O., Leipe, T., Vogt, C., & El'gygytgyn Science Party. (2013). Modern sedimentation patterns in Lake El'gygytgyn, NE Russia, derived from surface sediment and inlet streams samples. *Climate of the Past*, *9*(1), 135–148. https://doi.org/10.5194/cp-9-135-2013